OCT 1 7 1978

NOV 1 3 1985

NOV 1 3 1991
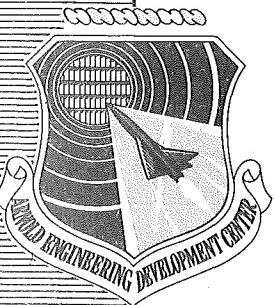
AN ANALYSIS
OF SECOND-THROAT DIFFUSER PERFORMANCE
FOR ZERO-SECONDARY-FLOW EJECTOR SYSTEMS

TECHNICAL REPORTS

FILE COPY

By

J. H. Panesci and R. C. German

Rocket Test Facility

ARO, Inc.

TECHNICAL DOCUMENTARY REPORT NO. AEDC-TDR-63-249

December 1963

Program Element 62405184/6950, Task 695002

(Prepared under Contract No. AF 40(600)-1000 by ARO, Inc.,
contract operator of AEDC, Arnold Air Force Station, Tenn.)

PROPERTY OF

AE

ARNOLD ENGINEERING DEVELOPMENT CENTER

AIR FORCE SYSTEMS COMMAND

UNITED STATES AIR FORCE

NOTICES

AN ANALYSIS

OF SECOND-THROAT DIFFUSER PERFORMANCE

FOR ZERO-SECONDARY-FLOW EJECTOR SYSTEMS

By

J. H. Panesci and R. C. German

Rocket Test Facility

ARO, Inc.

a subsidiary of Sverdrup and Parcel, Inc.

December 1963

ARO Project No. RW2141

ABSTRACT

A theoretical and experimental investigation was conducted to determine a method for predicting the starting pressure ratio for a zero-secondary-flow ejector system having a second-throat diffuser. The effects of second-throat contraction, location, and length on the ejector starting characteristics were investigated, and a method for predicting second-throat diffuser performance was developed using one-dimensional conservation equations. A comparison of both hot and cold flow data with the developed theory is presented. Good agreement between experiment and theory is obtained for both long and short second-throat diffusers. For example, the short second-throat theory deviated from the short second-throat experimental data by a maximum of 10.2 percent with an average deviation of 3.3 percent.

PUBLICATION REVIEW

This report has been reviewed and publication is approved.

Eules L. Hively
Acting Chief, Propulsion Division
DCS/Research

Donald R. Eastman, Jr.
DCS/Research

CONTENTS

TABLES

ILLUSTRATIONS

NOMENCLATURE

A	Area
C_f	Friction coefficient
D	Diameter
F	Force or impulse function
f	Friction force
I	Impingement
L	Length
M	Mach number
$\dot{m}$	Mass flow
p	Static pressure
p_t	Total pressure
q	Dynamic pressure
R	Gas constant
r	Radius from diffuser centerline
T_t	Total temperature
x	Axial distance
γ	Ratio of specific heats
θ	Angle

SUBSCRIPTS

1, 2, 3	Axial stations
c	Ejector cell
cal	Calculated
d	Duct
ex	Exhaust (same as station 3)
exp	Experimental
i	Impingement section
m	Ramp mid-area

n	Nozzle
ne	Nozzle exit
oper	Operate
opt	Optimum
R	Ramp section
s	Separated
sp	Spherical
st	Second throat
t	Total
w	Wall
x	Axial direction

SUPERSCRIPT

*	Nozzle throat

1.0 INTRODUCTION

The investigation of second-throat, ejector-diffuser (STED) systems reported in Ref. 1 showed that the diffuser pressure recovery of an ejector-diffuser system can be greatly increased when a second throat is employed. Application of this increase is of considerable interest in the design of ejector-diffuser systems for rocket test facilities where the ever increasing requirement for facilities to simulate higher altitude conditions is limited by the available cylindrical diffuser pressure recovery. It was also noted (Ref. 2) that a STED system would start at a second-throat contraction considerably greater than that allowed by the wind tunnel normal shock limitation.

Existing methods for sizing a second-throat diffuser have been limited to using an empirical limiting contraction curve developed in Ref. 2 by NASA. Also, available methods stated in Ref. 1 for calculating the starting pressure ratio for STED systems are as much as 50 percent in error. Since a rigorous analysis of the axisymmetric flow conditions within the diffuser is very difficult, a simple method has been developed for calculating second-throat diffuser performance. In addition, an experimental investigation of second-throat performance was made at the Rocket Test Facility (RTF), Arnold Engineering Development Center (AEDC), Air Force Systems Command (AFSC), during the period from January 7 to May 3, 1963, to obtain further information on the operation of second-throat diffusers to aid in the analysis of second-throat operation.

2.0 THEORETICAL ANALYSIS

A contracting diffuser section is the primary method which is used to reduce the overall pressure ratio required to operate a supersonic wind tunnel. This same principle may be applied to the rocket exhaust ejector-diffuser to increase the maximum exhaust pressure at which the ejector-diffuser may be started and operated. Before discussing the operation of STED systems, it is necessary to define a few terms which will be used throughout the report.

1. MINIMUM CELL PRESSURE is the cell pressure obtained from a given zero-secondary-flow, ejector-diffuser configuration when the cell pressure becomes independent of exhaust pressure (Fig. 1).

P27

Manuscript received November 1963.

2. EJECTOR STARTED is the condition that exists when the exhaust gases from the nozzle of a STED system pump a cell pressure approximately equal (± 10 percent) to the minimum cell pressure obtainable for a similar cylindrical diffuser.

3. SECOND-THROAT STARTED is defined as being the condition that exists when the Mach number at the entrance to the minimum area is greater than one and the cell pressure pumped by the nozzle exhaust gases is independent of the exhaust pressure. (Cell pressure may or may not be equal to minimum cylindrical cell pressure.) This condition corresponds to the wind tunnel normal-shock-swallowed condition.

4. SHORT SECOND THROAT is one in which the Mach number entering the minimum area is approximately equal to the Mach number leaving the minimum area during normal operation (usually $(L/D)_{st} < 1$).

5. LONG SECOND THROAT is defined as one which is long enough to allow approximately normal shock recovery from the Mach number entering the minimum area through a system of oblique shocks $(L/D)_{st} \gtrsim 5$.

2.1 SHORT SECOND-THROAT THEORY

For short second-throat diffusers, the maximum exhaust pressure at which the ejector may be started and operated can be determined by a straightforward application of the conservation equations between stations one and three.

2
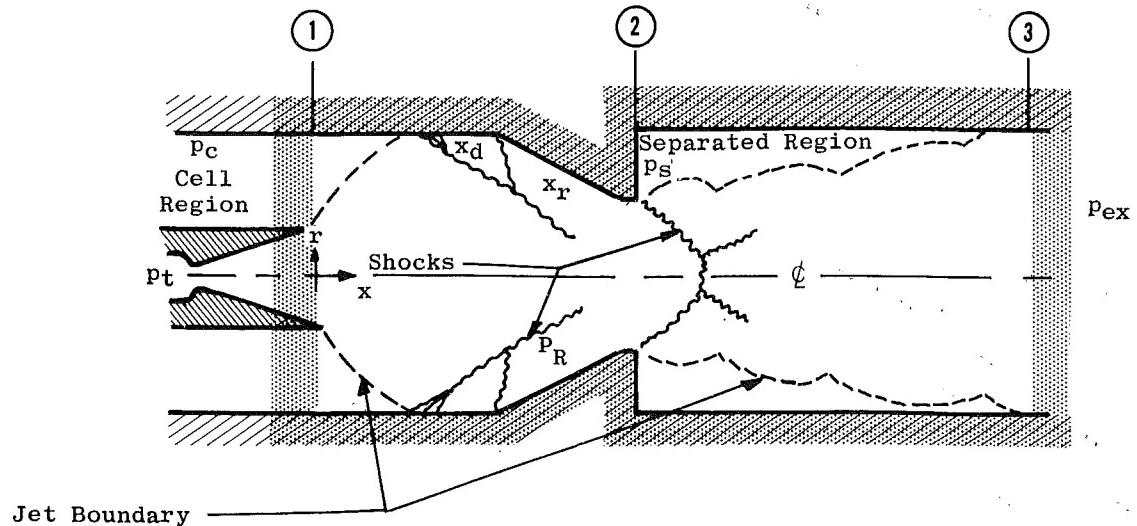
The following assumptions are made to simplify the solution of the conservation equations:

1. Flow is steady,

2. Gas is perfect,

3. Flow is adiabatic,

4. Flow is one dimensional at stations two and three,

5. Gas velocity in the cell region and the separated region aft of the second throat is zero,

6. The gas fills the diffuser at station three,

7. Friction losses in the minimum area are negligible, and

8. The static pressure at station three equals the exhaust pressure (p_{ex}).

The above assumptions are used in the following force balance made between stations one and two.

$$F_{ne_x} + p_c \pi (r_d^2 - r_{ne}^2) - f_d - f_{R_x} - \int_{r_{st}}^{r_d} p_R \frac{\sin\theta_{st}}{} \pi 2r \frac{dr}{\sin\theta_{st}} = p_2 \pi r_{st}^2 (1 + \gamma M_2^2) \tag{1}$$

The left hand side of this equation can be evaluated in several ways with varying degrees of accuracy. Although empirical methods are suggested for estimating these quantities in section 4.0, it is significant to note that the axial nozzle thrust (F_{ne_x}) and the pressure area integral on the second-throat ramp contribute the most to the magnitude of the terms on the left hand side of Eq. (1).

From continuity and energy considerations and using the previously stated assumptions, the following equation may be written:

$$\dot{m} \sqrt{R T_t} = p_2 \pi r_{st}^2 M_2 \sqrt{\gamma \left(1 + \frac{\gamma - 1}{2} M_2^2\right)} \tag{2}$$

Dividing Eq. (1) by Eq. (2), gives

$$\frac{F_{ne_x} + p_c \pi (r_d^2 - r_{ne}^2) - f_d - f_{R_x} - 2\pi \int_{r_{st}}^{r_d} p_R \, r \, dr}{\dot{m} \sqrt{R T_t}} = \frac{1 + \gamma M_2^2}{M_2 \sqrt{\gamma \left(1 + \frac{\gamma - 1}{2} M_2^2\right)}} \tag{3}$$

or

$$\frac{\Sigma_1^2 F}{\dot{m} \sqrt{R T_t}} = \frac{1 + \gamma M_2^2}{M_2 \sqrt{\gamma \left(1 + \frac{\gamma - 1}{2} M_2^2\right)}} \tag{3a}$$

3

If the left hand side of Eq. (3) can be calculated (see section 4.0), then for a given ratio of specific heats, γ, there exist two values of Mach number that satisfy the equation. Figures 2a and b present the graphical solution for these two Mach numbers for various values of gamma. Shapiro points out in Ref. 3 that the Mach number in the minimum area of a wind tunnel second throat must be supersonic when the tunnel is started (second throat started). Therefore, from this and experimental verification, the supersonic solution is found to be the correct value of M_2 for the ejector second-throat started condition. The value of M_2 obtained from Fig. 2b is used in Eq. (2) to calculate the static pressure in the second throat at station two (p_2). The maximum value of the pressure, p_s, that can exist in the separated region without unstarting the second throat by separating the flow in the minimum area may be determined from turbulent boundary-layer-free, shock-separation theory. Reference 4 suggests a relatively simple method for obtaining the relation between the separation static pressure rise, p_s/p_2, and the Mach number, M_2.[‡] When the value of p_s is known, the overall force balance can be made between stations one and three.

$$\frac{\Sigma_1^2 F + p_s \pi \left(r_{ex}^2 - r_{st}^2 \right)}{\dot{m} \sqrt{R T_t}} = \frac{1 + \gamma M_3^2}{M_3 \sqrt{\gamma \left(1 + \frac{\gamma - 1}{2} M_3^2 \right)}} \tag{4}$$

or

$$\frac{\Sigma_1^3 F}{\dot{m} \sqrt{R T_t}} = \frac{1 + \gamma M_3^2}{M_3 \sqrt{\gamma \left(1 + \frac{\gamma - 1}{2} M_3^2 \right)}} \tag{4a}$$

The value of M_3 in Eq. (4a) can then be determined by using the subsonic graphical solution (Fig. 2a). At station three, the subsonic solution is the solution of physical significance since: (1) the Mach number must decrease in the unfavorable (increasing) pressure gradient between stations two and three and (2) it allows the exhaust pressure to be a maximum. The maximum value of exhaust pressure, p_{ex}, at which the short second-throat ejector-diffuser may be started and operated can now be calculated by using the continuity equation.

$$p_{ex} = \frac{\dot{m} \sqrt{R T_t}}{A_3 M_3 \sqrt{\gamma \left(1 + \frac{\gamma - 1}{2} M_3^2 \right)}} \tag{5}$$

[‡] If the STED system is exhausting into a large volume or to atmosphere at station two, the value of the separation pressure, p_s, is the maximum exhaust pressure at which the second throat will start and operate.

4

2.2 LONG SECOND-THROAT THEORY

The maximum exhaust pressure at which the long second-throat diffuser will start and operate may also be determined by using the conservation equations.
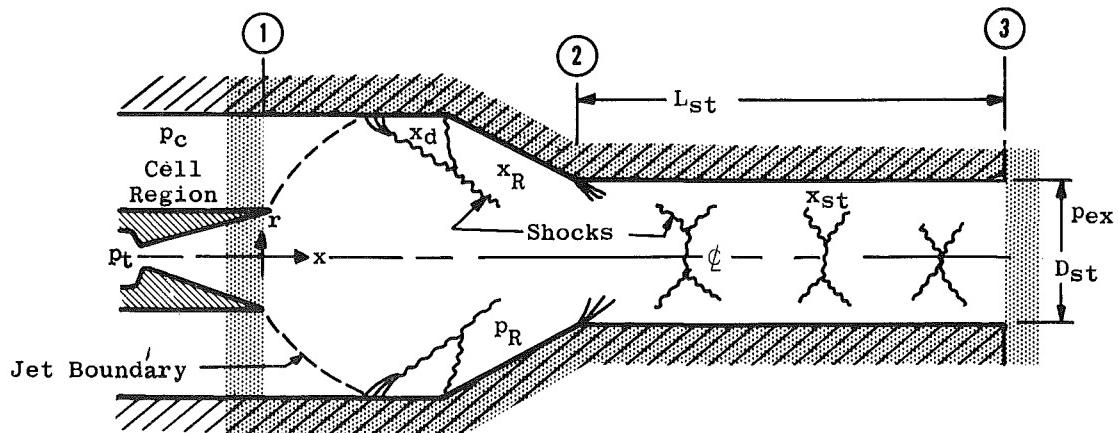
To simplify the solution of the conservation equations the following assumptions are made:

1. Flow is steady,

2. Gas is perfect,

3. Flow is adiabatic,

4. Flow is one dimensional at stations two and three,

5. Gas velocity in cell region is zero,

6. Friction losses in the minimum area may be estimated by assuming a linear Mach number distribution from station two to station three and a constant friction coefficient, and

7. The static pressure at station three equals the exhaust pressure, p_{ex}.

The force balance between stations one and two of the long second throat is identical to the force balance between stations one and two of the short second throat. Based on this and the above assumptions, the

overall conservation equations between stations one and three may be
written:

$$\frac{\sum_1^2 F - \int_2^3 d\,f_{st}}{\dot{m}\,\sqrt{R\,T_t}} = \frac{1 + \gamma\,M_3^2}{M_3\sqrt{\gamma\left(1 + \frac{\gamma-1}{2}M_3^2\right)}} \tag{6}$$

From Ref. 3,

$$d\,f_{st} = \frac{C_f\,p_{st}\,A_{st}\,\gamma\,M_{st}^2}{r_{st}}\,dx \tag{7}$$

and

$$\text{CONTINUITY} \quad \dot{m}\,\sqrt{R\,T_t} = p_{st}\,A_{st}\,M_{st}\,\sqrt{\gamma\left(1 + \frac{\gamma-1}{2}M_{st}^2\right)} \tag{8}$$

Equations (6), (7), and (8) are combined to give

$$\frac{\sum_1^2 F}{\dot{m}\,\sqrt{R\,T_t}} = \int_0^{L_{st}} \frac{C_f\,\gamma\,M_{st}}{r_{st}\sqrt{\gamma\left(1 + \frac{\gamma-1}{2}M_{st}^2\right)}}\,dx + \frac{1 + \gamma\,M_3^2}{M_3\sqrt{\gamma\left(1 + \frac{\gamma-1}{2}M_3^2\right)}} \tag{9}$$

The assumed linear Mach number distribution from stations two
to three is

$$M_{st} = \frac{x}{L_{st}}(M_3 - M_2) + M_2 \tag{10}$$

therefore,

$$d\,M_{st} = \left(\frac{M_3 - M_2}{L_{st}}\right)dx \tag{11}$$

Equation (9) may be rewritten by using Eqs. (10) and (11):

$$\frac{\sum_1^2 F}{\dot{m}\,\sqrt{R\,T_t}} = \frac{C_f\,\sqrt{\gamma}\,2\left(\frac{L_{st}}{D_{st}}\right)}{\sqrt{\frac{\gamma-1}{2}}\,(M_3 - M_2)}\int_{M_2}^{M_3}\frac{M_{st}}{\sqrt{\frac{2}{\gamma-1} + M_{st}^2}}\,d\,M_{st}$$

$$+ \frac{1 + \gamma\,M_3^2}{M_3\sqrt{\gamma\left(1 + \frac{\gamma-1}{2}M_3^2\right)}} \tag{12}$$

The integral in Eq. (12) is evaluated; thus

$$\frac{\Sigma_1^2 \, F}{\dot{m} \sqrt{R T_t}} = \sqrt{\frac{2\gamma}{\gamma - 1}} \quad \frac{C_f \, 2 \left(\frac{L}{D}\right)_{st}}{(M_3 - M_2)} \left[\sqrt{\frac{2}{\gamma - 1} + M_3^2} - \sqrt{\frac{2}{\gamma - 1} + M_2^2} \right]$$

$$+ \frac{1 + \gamma M_3^2}{M_3 \sqrt{\gamma \left(1 + \frac{\gamma - 1}{2} M_3^2\right)}} \tag{13}$$

The value of M_3 may then be determined from Eq. (13) by using Eq. (3) or Fig. 2b to find the value of the supersonic Mach number M_2. A graphical solution for M_3 is presented in Fig. 2a for $\gamma = 1.4$ $(L/D)_{st} = 8$ and $C_f = 0.008$. The maximum value of exhaust pressure, p_{ex}, at which the long second throat will start and operate may then be found from the continuity equation, Eq. (5).

Equation (13) and Fig. 2b may also be used to calculate the exit Mach number of a cylindrical ejector diffuser (no second throat). For this case, the force summation consists of only the axial nozzle thrust, F_{ne_x}, plus the cell pressure area term, $p_c(A_d - A_{ne})$.

2.3 STARTING LIMITATIONS

The starting characteristics of a STED system may be divided into second-throat starting and ejector starting. The starting of a second throat is similar to a wind tunnel normal shock swallowing process by which supersonic flow is established in the second throat. The ejector starting occurs after the second throat is started and is the process whereby the free-jet boundary expands and pumps a minimum cell pressure. The limitations of this process are similar to those of a variable area wind tunnel second throat. References 1 and 2 present data which indicate that the wind tunnel normal shock starting limitation is not valid for the ejector second-throat starting based on the fixed geometric contraction (A_{st}/A_d). This is demonstrated by Fig. 3 in which the wind tunnel normal shock starting limit is compared with an experimentally determined limiting contraction ratio curve (Ref. 2) for STED's. This apparent contradiction can be explained by the fact that for an ejector system, the cell pressure will automatically adjust the flow field so that the normal shock limit is not violated during second-throat starting.

The wind tunnel normal shock starting limit (Ref. 5) is based on the hypothesis that the second throat accepts the mass flow from the primary

throat with a maximum total pressure loss to the gas. These two considerations are expressed in the normal shock limiting equation:

$$\frac{A^*}{A_{st}} = \frac{P_{t_2}}{P_{t_1}} \tag{14}$$

where the total pressure ratio is the normal shock value at the maximum flow field Mach number.

The automatic adjustment concept may be demonstrated by considering what happens during starting of a STED if the normal shock limit is violated. If the wind tunnel normal shock limit is violated, more mass will be added to the system (to the cell) by the primary nozzle than is being allowed to pass through the second throat. This will result in an increase in cell pressure which will cause the maximum Mach number and area of the flow field to decrease. An oblique shock system is then set up in the flow field, and, if the nozzle is sufficiently close to the second throat, normal shock losses are no longer experienced. The second throat may then accept the mass flow from the nozzle and become started (shock swallowed).

After the second throat starts, the increase in the mass being pumped out of the cell causes a decrease in cell pressure with a corresponding increase in the maximum Mach number and effective second-throat area ratio. This action corresponds to that of a variable area wind tunnel wherein the second-throat contraction can be increased once the shock is swallowed. Cell pressure will continue to decrease until (1) the minimum force to mass flow ratio (choking) is reached in the second throat or (2) the minimum cell pressure is achieved. The experimental ejector-diffuser limit (Fig. 3) is a result of choking conditions being reached in the second throat.

3.0 EXPERIMENTAL INVESTIGATION

An experimental investigation of second-throat performance was made in support of the theoretical analysis. The ejector starting and operating characteristics were recorded, and the wall static pressure distributions in the second-throat were measured. Additional information on the effect of cylindrical diffuser diameter and second-throat length on second-throat performance was also obtained.

3.1 EXPERIMENTAL APPARATUS

Nine ejector-diffuser configurations were tested during the experimental investigation of second-throat performance. A 10.19-in. cylindrical diffuser with a second throat having a contraction ratio, $A_{st}/A_d = 0.438$, and a 12-deg ramp angle were selected for this investigation on a basis of the starting contraction limitation and second-throat performance reported in Ref. 1. Second-throat diffusers with various throat lengths were tested with four 18-deg conical nozzles whose area ratios varied from 3.63 to 25.0. A description of the nozzles and second-throat diffusers which were tested is given in Table 1.

3.1.1 Test Hardware Description

The nozzles were concentrically located in the cylindrical diffuser with the upstream end of the diffuser attached to a sealed plenum. A typical test configuration is shown in Fig. 4. The nozzles were mounted on a movable section of inlet supply pipe which permitted the nozzle to be translated approximately 9.0 in. along the horizontal centerline of the cylindrical diffuser. The design of the "O"-ring seals in the telescoping sections permitted the nozzle to be positioned during a test without leakage into the cell region. The position of the nozzle with respect to the second throat was indicated by a counter which registered the rotations of the actuating mechanism.

The code designation for the various ejector configurations (both nozzles and diffusers) is included in Table 1. A typical ejector configuration designation would be 4-5d, which indicates an 18-deg conical nozzle with an area ratio of 25.0 exhausting into a 10.19-in. cylindrical diffuser with a second-throat diffuser having a throat length to diameter ratio, $(L/D)_{st} = 8.1$, and a contraction ratio, $A_{st}/A_d = 0.438$.

3.1.2 Instrumentation

The parameters measured during this investigation were: cell pressure, p_c; exhaust pressure, p_{ex}; nozzle total pressure, p_t; static pressures along the second throat and cylindrical diffuser walls, p_w; static pressures on the second-throat ramp, p_R; and total temperature, T_t. Table 2 contains the range of the measured parameters and the type of measuring instrument used for each.

3.2 EXPERIMENTAL PROCEDURE

Prior to each test, the nozzle, test cell, and instrumentation lines were pressure checked to minimize the possibility of leakage. A vacuum

check was also made prior to each test to reduce the possibility of instrumentation leakage.

Inlet air was supplied from the RTF compressors at pressure, p_t, as high as 46 psia and at a temperature of approximately 80°F. The ejectors exhausted into the RTF exhaust machines, which provided pressures as low as 7 mm HgA. An electrically operated throttling valve in the exhaust ducting was used to control the exhaust pressure. The inlet supply pressure was manually controlled by a gate-type valve.

The maximum exhaust pressure, p_{ex}, at which the ejector became started was obtained for each configuration at a given nozzle position and total pressure, p_t, by decreasing the exhaust pressure until the cell pressure, p_c, reached a minimum value. The exhaust pressure was then increased until the ejector again became unstarted (where p_c started to increase) to determine the maximum operating exhaust pressure. This procedure was repeated at various nozzle positions to determine the effect of second-throat location on ejector second-throat diffuser performance.

3.3 DISCUSSION OF EXPERIMENTAL RESULTS

3.3.1 Ejector and Second-Throat Starting Characteristics

A cylindrical ejector-diffuser system has been defined as starting when the expanded free-jet boundary from the nozzle impinges on the diffuser walls such that the cell pressure becomes a minimum value for a given nozzle total pressure and is not affected by reductions in the exhaust pressure (Fig. 1). This same definition can be applied to ejector systems employing second-throat diffusers: however, as discussed in section 2.0, it is possible for the second throat to become started without having the ejector started (cell pressure not minimum). Since this condition occurs only when the optimum second-throat contraction is exceeded (Fig. 3), the starting of an ejector and a second throat can be assumed to be synonymous for an ejector, second-throat diffuser system which is properly designed. The effects of various second-throat parameters on the ejector and second-throat starting characteristics are discussed in the following paragraphs. A complete tabulation of the experimental results is presented in Table 3.

3.3.1.1 Effect of Second-Throat Contraction

One of the most important factors which must be considered during the design of a second-throat diffuser is the contraction ratio. Figure 5

shows a comparison of the maximum second-throat contraction curves presented in Ref. 2 with the experimental data obtained during this investigation and the data previously reported in Ref. 1. The effect of a properly located second throat on minimum cell pressure is relatively insignificant as long as this maximum contraction is not exceeded. Reference 1 shows, however, that the second throat should be designed as close to the maximum contraction as possible for maximum efficiency (maximum p_{ex}/p_c). The theoretical method for determining this maximum contraction for conical nozzle configurations is presented in section 5.2.

3.3.1.2 Effect of Second-Throat Length and Location

The location of the second-throat not only affects the starting pressure ratio but also can affect cell pressure if improperly located (see Fig. 6). When the second throat is positioned too far upstream, the free jet impinges upon the ramp, causing the cell pressure to increase. When a second throat is positioned too far downstream, the ejector will not start because of the decrease in Mach number entering the second throat. Figure 7 shows the experimental static pressure distribution immediately upstream of the second throat and on the inlet ramp for various second-throat positions. A probable flow model of the gas entering the second-throat diffuser is also shown in Fig. 7 for $x_{st}/D_d = 0.80$.

Figure 8 shows the effect of second-throat position on the ejector starting characteristics for various throat lengths. This figure along with Fig. 9 illustrates the importance of positioning the second throat in some optimum location. This optimum location should be such that free-jet impingement is upstream of the second-throat ramp for second throats of all lengths. However, the exact second-throat position is not as critical for either short $\left[(L/D_{st} \leq 1\right]$ or long $\left[(L/D)_{st} = 8\right]$ throats as it is for intermediate length second throats as is shown in Fig. 9. It should be realized that the increase in the starting pressure ratio, p_{ex}/p_t, shown in Fig. 9 at the intermediate throat lengths is due to the subsonic diffuser action downstream of the minimum area section. This would indicate that the most efficient second-throat geometry for an available diffuser length could be an intermediate length second throat with a subsonic diffuser. Further study is required to evaluate this type of diffuser. In the calculation of the starting pressure ratio, the pressures on the ramp of the second throat are of great importance. It is, therefore, important to note in Fig. 10 that the pressure distributions on the ramps of otherwise identical geometric long and short second-throat ejector-diffusers are the same.

Most zero flow ejector systems are operated with the ejector started. However, one method of testing a given rocket motor at

several altitude conditions with one ejector system would be to oper-
ate the ejector in the unstarted regions where cell pressure is higher.
The feasibility of such an operation would greatly depend upon the
stability of the ejector when it is unstarted. Figure 11 indicates that
instability may occur in a second-throat diffuser with an intermediate
throat length. This characteristic is similar to that reported in
Refs. 6 and 7 for cylindrical diffuser systems when the diffuser length
was decreased.

3.3.2 Effect of Second Throat on Cell Pressure

Figure 6 shows the variation in ejector performance with and with-
out a second throat. These data and those presented in Ref. 1 indicate
that the minimum cell pressure can be influenced by the presence of a
second throat even if the impingement point is well upstream of the
second-throat ramp. A possible explanation of why a second throat
affects minimum cell pressure is given in the Appendix.

4.0 CALCULATION PROCEDURE

The calculation of both short and long second-throat diffuser per-
formance requires the evaluation of Eqs. (3) and (13), respectively.
There are various methods and assumptions that can be made to solve
for the individual forces in these force balances. In the following dis-
cussion, the techniques used to evaluate all the performance data pre-
sented in this report are reviewed. These methods are not necessarily
the best or most accurate; however, as will be shown by comparison
with the experimental data (section 5.0), they do suffice for the vast
majority of the conditions. Particular attention will be given to the
axial nozzle thrust, the ramp pressure area term, and the short second-
throat separation pressure rise since these quantities are at least an
order of magnitude greater than the friction and cell pressure force
terms.

4.1 NOZZLE THRUST

The axial thrust of the conical nozzles was calculated by assuming
a spherical Mach number distribution at the nozzle exit. The effective
spherical area ratio of the nozzle may then be related to the geometric
(plane) area ratio by

$$\frac{A_{sp}}{A^*} = \left(\frac{2}{1 + \cos\theta_{ne}}\right) \frac{A_{ne}}{A^*} \tag{15}$$

where

θ_{ne} is the nozzle exit half angle. The gas is then assumed to expand isentropically from the plane throat area to the spherical exit area. The axial nozzle thrust may then be determined from

$$F_{ne_x} = A_{ne} \, P_{sp} \, (1 + \gamma \, M_{sp}^2) \tag{16}$$

where the pressure and Mach number are based on the spherical area ratio and the nozzle exit area is the plane area. A complete derivation of this method may be found in Ref. 8.

4.2 RAMP PRESSURE AND RAMP FRICTION

The most difficult terms to evaluate in the second-throat momentum balance are the pressure area and friction forces on the second-throat ramp. As mentioned previously, the pressure area term is considerably larger than the friction term; therefore, it is the most critical. Various unsuccessful methods were tried, including a rigorous characteristic network, before the following simplified method proved satisfactory. This method assumes that the gas expands isentropically from the nozzle throat to the diffuser duct diameter with the mean gas expansion angle (θ_m) being determined by the following geometric equation (see Fig. 12):

$$\theta_m = \tan^{-1} \left(\frac{r_m}{x_n + x_{st} + x_m} \right) \tag{17}$$

or

$$\theta_m = \tan^{-1} \left[\frac{\sqrt{\dfrac{A_{st}}{A_d} + 1}}{2 \sqrt{2} \left(\dfrac{x_n}{D_d} + \dfrac{x_{st}}{D_d} \right) + \dfrac{\sqrt{2} - \sqrt{\dfrac{A_{st}}{A_d} + 1}}{\tan \theta_{st}}} \right] \tag{17a}$$

The gas is then assumed to turn parallel to the second-throat ramp through a single oblique shock. The one-dimensional Mach number (isentropic function of $A_d/A*$ and γ) and the gas total turning angle θ_t (mean gas expansion angle plus ramp angle) are then used to obtain the conditions on the second-throat ramp from two-dimensional oblique shock considerations.

get Pr from oblique shock analysis

In Figs. 13a, b, and c the results of this method are compared with experimental pressure coefficients measured from three nozzle second throat configurations, each at three second-throat locations, x_{st}.

13

The ramp pressure integral from Eq. (3) may now be evaluated by assuming that p_R is independent of radius, r.

$$2\pi \int_{r_{st}}^{r_d} p_R \, r \, dr = p_R \pi (r_d^2 - r_{st}^2) \tag{18}$$

The ramp friction term may also be evaluated by using the pressure and Mach number obtained downstream of this single oblique shock.

$$f_{R_x} = \cos \theta_{st} \frac{\gamma \, C_f}{2} p_R M_R^2 A_R \tag{19}$$

or

$$f_{R_x} = \frac{\gamma \, C_f}{2} p_R M_R^2 \pi (r_d^2 - r_{st}^2) \cot \theta_{st} \tag{19a}$$

For all calculations made in this report, a constant friction coefficient, C_f, of 0.003 is assumed.

4.3 CELL PRESSURE AND DUCT FRICTION

The cell pressure area term was estimated by assuming that the gas expands isentropically from the nozzle throat to the duct area. Cell pressure is then assumed to be equal to the static pressure of the flow field at the duct wall. This method may be considerably in error; however, because of the relatively small magnitude of this term, the overall accuracy of the force balance is not impaired.

If the second throat is located at or near its optimum position, the duct friction term will be very small. If, for some reason, the second throat must be located considerably downstream from its optimum location, the duct friction loss may become significant. The duct friction was estimated by assuming a constant Mach number, static pressure, and friction coefficient ($C_f = 0.003$) from the free-jet impingement point to the inlet to the second-throat ramp. The Mach number and static pressure at the duct wall were estimated by assuming that the gas turns parallel to the wall from the free-jet boundary through a single oblique shock. The free-jet impingement angle (gas turning angle) and location were calculated using the method described in Ref. 9, by assuming the same value of cell pressure used to calculate the cell pressure area force term. The Mach number upstream of the oblique shock was assumed to be the one-dimensional duct Mach number M_d (function of

$\frac{A_d}{A*}$). Duct friction was then determined from

$$f_d = \pi \gamma C_f p_w M_w^2 r_d (x_{st} - x_i) \tag{20}$$

where the pressure and Mach number are those downstream of an oblique shock.

4.4 SEPARATION PRESSURE RATIO

The boundary layer free shock separation pressure ratio, p_s/p_2 for the short second-throat calculations was determined using the method suggested in Ref. 4. This method was used to calculate the static pressure rise ratio for various values of the ratio of specific heats as a function of upstream Mach number (see Fig. 14). Separation pressure was measured for eight ejector start points, compared with the calculated values, and found to have an average deviation of about 7.5 percent.

5.0 EXPERIMENTAL VERIFICATION OF THEORY

The value of this theoretical method depends upon its agreement with experimental results. For this reason, the cold flow data from Ref. 1 and the hot flow data from Ref. 10 were compared with the theory along with the results obtained during this experimental investigation.

5.1 STARTING PRESSURE RATIO

5.1.1 Short Second Throats

In Figs. 15 a-f the experimental ejector starting pressure ratios are compared with the theoretical method discussed in section 2.1. The theoretical values were calculated using the techniques outlined in sections 4.1.1 through 4.1.3. Sixteen nozzle second-throat combinations, each at four second-throat locations, were evaluated. Good agreement is obtained for all configurations except for 1-4a (Fig. 15e) taken from Ref. 1. It was pointed out in this reference that for this configuration the flow probably separated upstream of the second-throat ramp, producing a smaller ramp pressure area term. Excluding configuration 1-4a the remaining 59 points had a bias deviation[†] of -0.66 percent

---

[†]Bias Deviation = $\dfrac{\sum_1^{\eta} \% \text{ Deviation}}{\eta}$ where η = number of configurations.

and a maximum deviation of from -10.2 to +9.2 percent with a most probable deviation[†] for a single calculation of 2.8 percent.

5.1.2 Long Second Throats

5.1.2.1 Cold Flow

The long second-throat theory (section 2.2) is compared with experimental start points for 5 nozzle second-throat combinations in Figs. 16a and b. Unfortunately the experimental start pressures used for Fig. 16a were measured downstream of the second-throat exit. The closed symbols in this figure were calculated by assuming that the gas expanded subsonically from the second-throat exit and filled the concentric duct. The data in Fig. 16a indicate that the gas actually expanded to a diameter somewhere between the second-throat exit and the concentric duct diameter. The long second-throat theory deviated from the experimental data used for Fig. 16b by an average of 4.4 percent.

5.1.2.2 Hot Flow Correlation

The experimental results obtained from Ref. 10 for $\gamma = 1.3$ and 1.22 are compared with the long and short second-throat theories in Figs. 17a and b. This limited comparison indicates that the starting pressure ratio for hot flow STED systems can be calculated to within 10 percent for throat lengths greater than $(L/D)_{st} = 8$. No hot flow experimental results were available for comparison at throat lengths, $(L/D)_{st} < 1.0$.

5.1.2.3 Cylindrical Diffuser Performance

The long second-throat theory may also be used to calculate cylindrical duct diffuser performance. The cylindrical diffuser starting pressure ratio may be calculated by using Eq. (13) where the force summation is nozzle exit thrust plus the cell-pressure-area term. This was done for six configurations and compared with the experimental values (Fig. 18). The theory deviated from the experimental data by an average of 0.63 percent with a maximum deviation of 1.69 percent.

5.1.3 Intermediate Length Second Throats

The methods which have been developed for calculating the ejector starting pressure ratio cannot be applied directly to second-throat

---

[†] Most Probable Deviation $= \dfrac{\sum_{i}^{\eta} \left| \% \text{ Deviation} \right|}{\eta} \times 0.8453$

diffusers having intermediate throat lengths $\left[1.0 < (L/D)_{st} \leq 5.0\right]$. Figure 19 shows an empirical correction which could be applied to the long throat theory to calculate the intermediate length second-throat starting pressure ratios for the one configuration investigated. The minimum second-throat length at which the long throat theory can be applied appears to be a function of the nozzle contour and exit angle. The starting pressure ratio for the 18-deg conical nozzle begins to decrease at $(L/D)_{st} = 4$ as shown in Fig. 19. For the 12.8-deg contour nozzles (Figs. 17a and b), the decrease begins at a throat length of approximately $(L/D)_{st} = 6$ to 8. This trend should be considered as preliminary until more information is obtained.

5.2 SECOND-THROAT GEOMETRIC LIMITS

The experimental second-throat contraction limit (Fig. 3) may be estimated from a force balance. This was done for short and long second-throats by solving Eqs. (3) and (13), respectively. At the choking condition, the right hand side of Eqs. (3) and (13) are equal to 1.85 and 1.90 for a ratio of specific heats of 1.4 (Figs. 2a and b). To facilitate the solution of these equations, the nozzle thrust and cell pressure area force are summed together as a function of the one-dimensional duct Mach number and static pressure (isentropic function of A_d/A^* and γ). The duct and ramp friction terms were not considered because they are both very small compared with the other terms. The ramp pressure area term was estimated by assuming that the gas turned through an angle of 35 deg through a single oblique shock (see discussion section 4.1.2). The results of this exercise are compared with the experimentally determined ejector limit curve in Fig. 3 and found to agree fairly well considering the simplicity of the calculation.

The force-to-mass flow ratio (Eq. 3) was calculated for 21 short second-throat ejector configurations. These calculations were made by assuming that the nozzle was at or near its optimum location (x_{st}/D_d) and that the cell pressure contribution to force was zero. This was plotted (Fig. 20) versus the ratio of the geometric area of the second throat to the minimum second-throat area allowable according to the empirical limit (Ref. 2). Figure 20 shows that only one configuration violated both the empirical and theoretical ejector starting limit. Careful analysis of the pressure data taken with this configuration (Ref. 1) suggests that, probably, the minimum cell pressure was not achieved because of a cell leak. Two additional configurations violated the theoretical ejector starting limit by not reaching minimum cell pressure. The one geometric factor uniquely common to both these configurations is a nozzle exit diameter larger than the second-throat diameter. This

may indicate a limit of applicability of the simplified ramp pressure method discussed in section 4.2.

It was pointed out in section 2.3 that if the nozzle is located sufficiently close to the second throat, the normal shock starting limit is automatically averted. A theoretical analysis of just how close the nozzle must be to the second throat is at best difficult; therefore, an empirical analysis was made. Figure 21 presents the start points farthest downstream for both long and short second throats versus the geometric second-throat area ratioed to the empirical minimum second-throat area (Fig. 3). As may be seen from the figure, the second-throat location becomes quite critical as the second-throat area approaches the optimum value. As expected, no maximum downstream start location was found for the three configurations which did not exceed the normal shock contraction limit.

6.0 CONCLUSIONS

The following conclusions are made from this investigation of second-throat, ejector-diffuser operation:

1. A method was developed for calculating long and short second-throat diffuser performance, which gives good agreement with experimental results.

2. The starting pressure ratio of 59 short second-throat ejector-diffuser configurations was calculated and found to deviate from the experimental starting pressure ratio by an average of 3.3 percent.

3. The starting pressure ratio of 12 long second-throat ejector-diffuser configurations was calculated and found to deviate from the experimental starting pressure ratio by an average of 4.4 percent.

4. The method developed for determining second-throat diffuser performance may also be applied to hot flow configurations.

5. The method developed for calculating the starting pressure ratio of long second-throat diffusers was used to calculate the starting pressure ratio of 6 cylindrical diffusers with the results deviating from the experimental data by an average of 0.6 percent.

6. The wind tunnel normal shock starting limit does not apply to the second-throat ejector-diffuser starting contraction when the second-throat is located at or near its optimum position.

7. The second-throat ejector-diffuser contraction is limited by choking conditions in the minimum area of the second-throat and may be estimated by a force balance.

8. The location of the second throat becomes more critical at the intermediate throat lengths. The optimum second-throat location for the intermediate lengths is immediately downstream of free-jet impingement.

9. There is a strong possibility that ejector instability will be encountered when an intermediate length second-throat ejector-diffuser is operated unstarted.

REFERENCES

1. Bauer, R. C., and German, R. C. "The Effect of Second-Throat Geometry on the Performance of Ejectors without Induced Flow." AEDC-TN-61-133, November 1961.

2. Jones, W. L., Price, H. S., and Lorenzo, C. F. "Experimental Study of Zero-Flow Ejectors Using Gaseous Nitrogen." NASA-TN-D-203, March 1960.

3. Shapiro, A. H. The Dynamics and Thermodynamics of Compressible Fluid Flow. Vol. I, pp 146, 165. The Ronald Press Co., New York, 1953.

4. Arens, M. and Spiegler, E. "Boundary Layer Separation in Over-Expanded Conical Exhaust Nozzles." AIAA Journal, Vol. I, pp 578-581, March 1963.

5. Liepmann, H. W. and Roshko, O. Elements of Gasdynamics. pp 133-136. John Wiley & Sons, Inc., New York, 1957.

6. German, R. C., Panesci, J. H., and Clark H. K. "Zero Secondary Flow Ejector-Diffuser Performance Using Annular Nozzles." AEDC-TDR-62-196, January 1963.

7. Barton, D. L. and Taylor, D. "An Investigation of Ejectors without Induced Flow, Phase I." AEDC-TN-59-145, December 1959.

8. Landsbamm, E. M. "Thrust of a Conical Nozzle." ARS Journal, Vol. 29, No. 3, pp 212-213. March 1959.

9. Latvala, E. K. and Anderson, T. P. "Experimental Determination of Jet Spreading from Supersonic Nozzles at High Altitudes." AEDC-TN-58-98, January 1959.

10. Roschke, E. J., Massier, P. F., and Gier, H. L. "Experimental Investigation of Exhaust Diffusers for Rocket Engines." Jet Propulsion Laboratory TR 32-210, March 1962.

11. Emmons, H. W. Fundamentals of Gas Dynamics, High Speed Aerodynamics and Jet Propulsion. Vol. III, Princeton University Press, 1958. Sec. B. "One-Dimensional Treatment of Steady Gas Dynamics." by L. Crocco, p 291.

12. Korst, H. H., Chow, W. L., and Zumwalt, G. W. "Research on Transonic and Supersonic Flow of a Real Fluid at Abrupt Increases in Cross Section." ME Technical Report 392-5, University of Illinois.

13. Chapman, D. R., Kuehn, D. M., and Larson, H. K. "Investigation of Separated Flows in Supersonic and Subsonic Streams with Emphasis on the Effect of Transition." NACA Report 1356, 1958.

APPENDIX
AN ANALYSIS OF THE INFLUENCES
OF SECOND-THROAT DIFFUSERS ON MINIMUM CELL PRESSURES

According to Crocco in Ref. 11, it is possible for the "dead water" region (or cell region) not to be isolated from downstream effects. Schlieren pictures in Ref. 11 show clearly that shocks in the region of free-jet impingement do not reach the wall. Crocco points out that this is because of the presence of subsonic flows in the boundary layer along the diffuser wall and in the zone where the jet mixes with the gases recirculating in the cell region. Crocco further states that these subsonic regions are thin, and if their longitudinal extent is sufficient, a disturbance downstream would influence the pressure in the cell region. A disturbance by a second throat could cause either an increase or a decrease in cell pressure if the mixing zone is initially laminar; however, if the mixing zone is initially turbulent, only an increase in cell pressure would be anticipated.

The increase in cell pressure can be explained when the mixing zone is initially laminar by considering a relation of the mass flows entrained and rejected in the cell region with the pressure differential, $p_i - p_c$, discussed in Refs. 12 and 13. When the point of transition from laminar to turbulent flow in the subsonic region is downstream of impingement as shown in the following illustration, an initial increase in $p_i - p_c$ results in a temporary increase in the mass flow rejected into the cell region. This causes an increase in cell pressure to establish equilibrium.

Transition Downstream of
Impingement (Steady State)
$m_e = m_r$

Initial Effect of Transition
Upstream of Impingement $m_e > m_r$

21
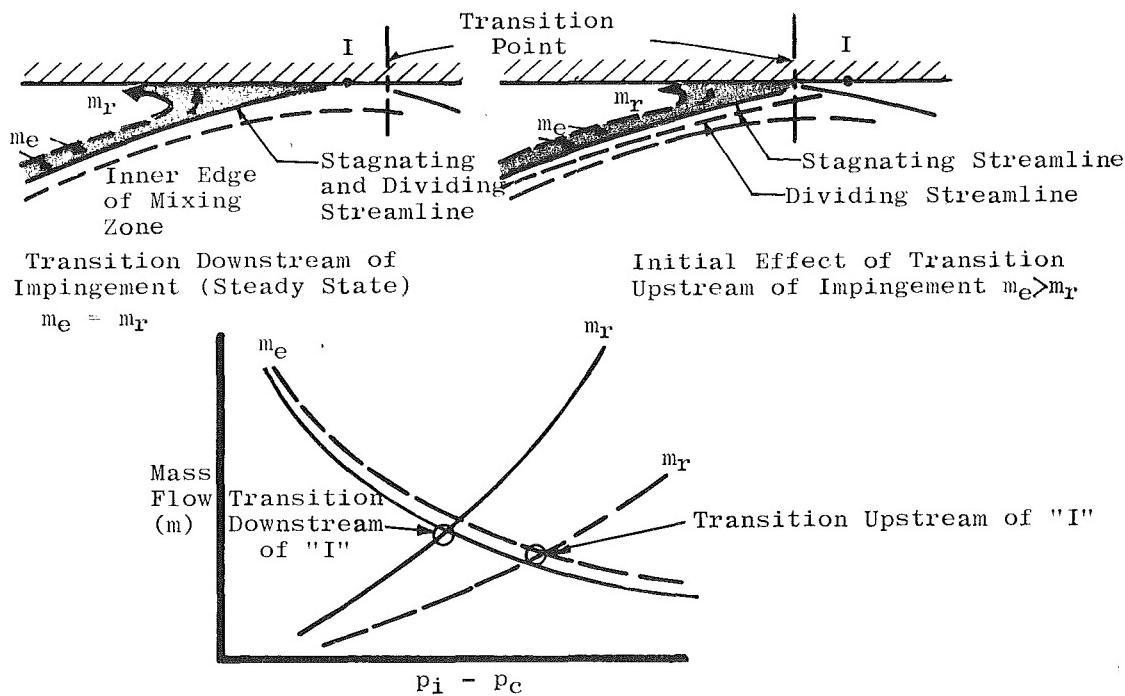
An increase in cell pressure will also occur when the peak static pressure, p_i, at the jet impingement point is increased because of an increase in the gas turning angle as a result of a downstream disturbance.

When the point of transition from laminar to turbulent flow moves upstream of free-jet impingement, turbulence moves upstream into the lower velocity portion of the mixing layer. If it is assumed that the mixing zone is laminar, this increases the velocity between the dividing streamline and the outer edge of the mixing zone such that the dividing streamline must move downstream of the stagnating streamline to satisfy continuity relations (see Ref. 12). Initially, this causes only a slight increase in the mass flow entrained since the length of the mixing layer along the dividing streamline is not decreased appreciably. However, the rejected mass flow would be decreased because of the turbulence which energizes the fluid particles in the low velocity portion of the mixing layer and enables more of them to overcome the pressure rise through the impingement zone. Thus, the amount of gas reversed is reduced for a given $p_i - p_c$, when the transition point moves upstream of jet impingement, and cell pressure must decrease to establish equilibrium, with a resulting decrease in the entrained mass flow. Although the manner in which transition is influenced by a second throat is not understood, the effect of transition on cell pressure provides an explanation of the decrease in cell pressure noted in Ref. 1 for the low Reynolds number data.

TABLE 1

DESCRIPTION OF COLD FLOW NOZZLES AND SECOND THROATS

Nozzle Dimensions				
Config. Code	$A_{ne}/A*$	$A*$, in.^{2}	D_{ne}, in.	θ_{ne}, deg
1†	3.63	3.799	4.19	18
3†	10.85	1.251	4.16	18
4†	25.00	0.542	4.16	18
5†	23.68	0.636	4.38	0
8	18.57	0.754	4.21	18

Second-Throat Dimensions				
Config. Code	A_{st}/A_d	θ_{st}, deg	A_d, in.^{2}	$(L/D)_{st}$
1a†	.654	6	28.463	0.43
2a†	.800	12	28.463	0.34
2b†	.568	12	28.463	0.33
3a†	.500	12	28.463	0.69
3b†	.500	12	28.463	8.00
3c†	.398	12	28.463	0.52
4a†	.654	18	28.463	0.38
5a	.438	12	81.553	0.55
5b	.438	12	81.553	3.00
5c	.438	12	81.553	5.00
5d	.438	12	81.553	8.10

†Same code as Ref. 1
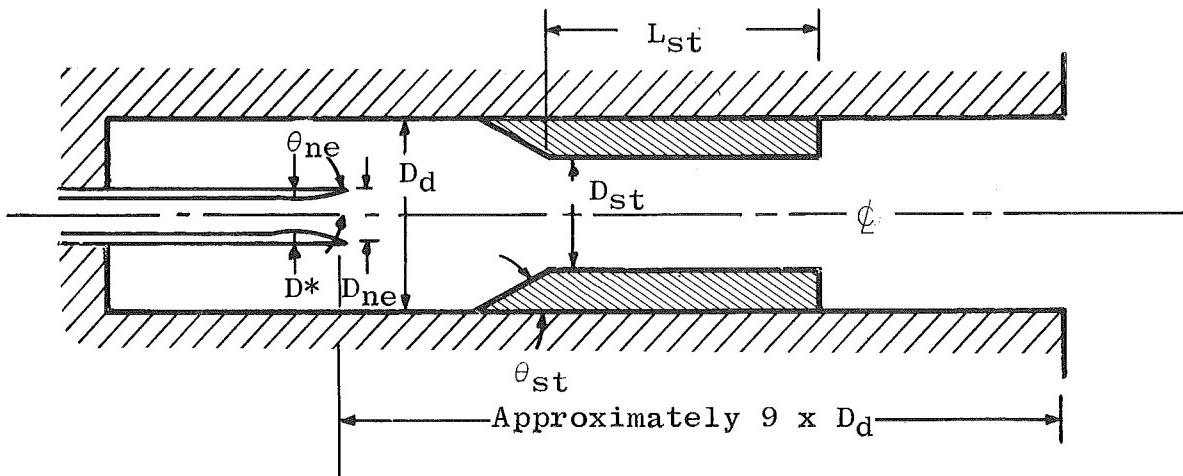
TABLE 2

DESCRIPTION OF MEASURING INSTRUMENTS

Parameter Measured	Range Measured	Measuring Instrument
p_c	0.2 to 5 mm HgA	McLeod (with nitrogen cold trap)
	5 to 50 mm HgA	Diaphragm-Activated Dial Gage
p_{ex}, p_{st}, and p_S	7 to 50 mm HgA	Diaphragm-Activated Dial Gage
	1 to 10 psia	Diaphragm-Activated Dial Gage
p_t	1 to 46 psia	Diaphragm-Activated Dial Gage
p_W or p_R	0.1 to 90 in. Oil	Manometer (silicone oil - sp. gr. = 1.092 at 80°F)
T_t	70 to 100°F	Copper Constantan Thermocouple

TABLE 3

SUMMARY OF TEST DATA

Config. Code	$(L/D)_{st}$	x_{st}/D_d	p_t, psia	p_c/p_t	p_{ne}/p_t	p_{st}/p_t† Start	p_{st}/p_t† Oper	p_{ex}/p_t‡ Start	p_{ex}/p_t‡ Oper	Remarks
1-5d	8.1	0.6716	40.19	.01257	.000623	---	---	---	---	Ejector would not start
1-5d		1.2912	39.99	.01573	.000641	---	---	---	---	
3-5d		0.6716	45.29	.000554	---	.0269	.0269	.0269	.0269	Ejector Started
		0.7337	45.29	.000560	---	.0280	.0280	.0280	.0280	
		0.7956	45.09	.000561	---	.0285	.0285	.0285	.0285	
		0.8575	45.19	.000569	---	.0290	.0290	.0290	.0290	
		0.9194	44.88	.000603	---	.0296	.0296	.0296	.0296	p_c increased
		0.09815	45.19	.000578	---	.0292	.0292	.0292	.0292	p_c increased
		1.0079	44.88	.000560	---	.0294	.0294	.0294	.0294	
3-5d		1.074	45.19	.00257	---	---	---	---	---	Ejector would not start
4-5d		0.6791	44.88	.000474	.00147	.0144	.0144	.0144	.0144	Jet impinged on ramp*
		0.8018	44.88	.000293	.00139	.0136	.0136	.0136	.0136	Ejector started
		0.9244	44.88	.000293	.00138	.0140	.0140	.0140	.0140	
		1.0471	44.88	.000293	.00138	.0142	.0142	.0142	.0142	
		1.1698	44.88	.000293	.00139	.0143	.0143	.0143	.0143	
		1.290	44.98	.000301	.00135	.0147	.0147	.0147	.0147	
4-5d		1.3538	44.88	.000293	.00139	.0147	.0147	.0147	.0147	
8-5d		0.672	44.93	.000517	.00195	.0182	.0183	.0182	.0183	Jet impinged on ramp*
		0.796	45.09	.000378	.00195	.0184	.0185	.0184	.0185	Ejector started
		0.919	44.98	.000378	.00195	.0190	.0190	.0190	.0190	
		1.043	44.98	.000378	.00195	.0190	.0190	.0190	.0190	
		1.167	44.98	.000387	.00195	---	---	---	---	
		1.191	44.98	.000408	.00195	.0193	.0193	.0193	.0193	p_c increased
8-5d	8.1	1.291	44.93	.001894	.00252	---	.0172	---	.0172	Ejector would not start
3-5c	5.0	0.620	44.29	.001653	---	---	---	---	---	Jet impinged on ramp*
		0.622	44.59	.000560	---	.02355	.02377	---	---	Ejector started
		0.679	44.39	.000558	---	.02636	.02659	.03019	.03053	
		0.740	44.33	.000560	---	---	.02786	---	.03203	
			44.29	.000561	---	---	.02823	---	.03225	
			44.29	.004813	---	---	.03048	---	.03477	Ejector intentionally unstarted for p_{ex} traverse
			44.39	.009097	---	---	.03717	---	.04107	
			44.33	.006435	---	---	.04218	---	.04563	
3-5c	5.0	0.740	44.33	.009812	---	---	.04443	---	.04883	

† p_{st} is measured in the second throat at the end of the minimum area section.
‡ p_{ex} is measured downstream of the second throat in the 30-in. -diam duct.
* p_s is measured immediately downstream of the minimum area section in the 10-in. diffuser.

TABLE 3 (Concluded)

Config. Code	$(L/D)_{st}$	x_{st}/D_d	p_t, psia	p_c/p_t	p_{ne}/p_t	p_{st}/p_t† Start	p_{st}/p_t‡ Oper	p_{ex}/p_t‡ Start	p_{ex}/p_t‡ Oper	Remarks
3-5c	5.0	0.740	44.33	.01623	---	---	.05481	---	.05594	Ejector intentionally unstarted for p_{ex} traverse
			44.33	.02176	---	---	.05930	---	.05930	
			44.33	.014890	---	---	.05312	---	.05474	
			44.33	.008130	---	---	.04207	---	.04669	
			44.29	.006617	---	---	.04065	---	.04437	
			44.29	.004104	---	---	.02890	---	.03365	
		0.740	44.29	.000561	---	.02800	---	.03188	---	Ejector started
		0.802	44.39	.000561	---	.02865	.02887	.03271	.03293	
		0.924	44.43	.000542	---	.02869	.02881	.03308	.03353	
3-5c	5.0	1.007	44.39	.000559 / .001216	---	---	---	---	---	Ejector unstarted at this point
3-5b	3.00	0.740	45.19	.000552	---	---	---	---	.01532	Ejector started
			45.19	.000552	---	---	---	---	.02351	
			45.19	.000552	---	---	---	---	.03057	
			45.19	.000552	---	---	.02572	---	.0318	Ejector intentionally unstarted for p_{ex} traverse
			45.19	.002821	---	---	---	---	.03256	
			45.19	.007192	---	---	---	---	.03738	
			45.19	.014687	---	---	---	---	.04960	
			45.19	.018334	---	---	---	---	.05411	
			45.19	.011781	---	---	---	---	.04575	
		0.740	45.19	.000552	---	.02572	---	---	---	Ejector started
		0.802	45.09	.000531	---	.02533	.02544	.03172	.03172	
		0.863	45.09	.000531	---	.02291	.02336	.03083	.03105	
		0.924	45.23	.000530	---	.02052	.02060	.02984	.02984	
3-5b	3.00	0.986	45.17	.000561	---	.01802	.01832	.02878	.02790	
3-5a	0.55	0.714	44.93	.000559	---	p_s*/p_t Start / .0169	p_s*/p_t Oper / .0175	--- / .0256	--- / .0256	
		0.740	44.93	.000551	---					
		0.768	44.83	.000560	---	---	---	---	---	
		0.802	44.93	.000551	---	.0170	.0177	.0254	.0254	
		0.826	44.83	.000552	---	---	---	---	---	
		0.839	44.88	.000543	---	---	---	---	---	
		0.851	44.88	.000534	---	---	---	---	---	
		0.863	44.98	.000537	---	.0154	.0157	.0246	.0247	
		0.924	44.88	.000538	---	.0153	.0155	.0247	.0247	
		0.986	44.83	.000604	---	.0139	.0140	.0232	.0232	p_c increased
3-5a		1.002	44.83	.00148	---	.0113	.01174	.0212	.0215	Ejector would not start
4-5a		0.768	44.54	.000299	---	.00648	.00665	.0115	.0117	Ejector started
		0.862	44.49	.000295	---	.00649	.00666	.0115	.0121	
		0.924	44.49	.000291	---	.00614	.00636	.0114	.0116	
		0.986	44.49	.000291	---	.00593	.00614	.0113	.0117	
4-5a	0.55	1.108	44.49	.000290	---	.00649	.00649	---	.0118	

† p_{st} is measured in the second throat at the end of the minimum area section.
‡ p_{ex} is measured downstream of the second throat in the 30-in.-diam duct.
* p_s is measured immediately downstream of the minimum area section in the 10-in. diffuser.
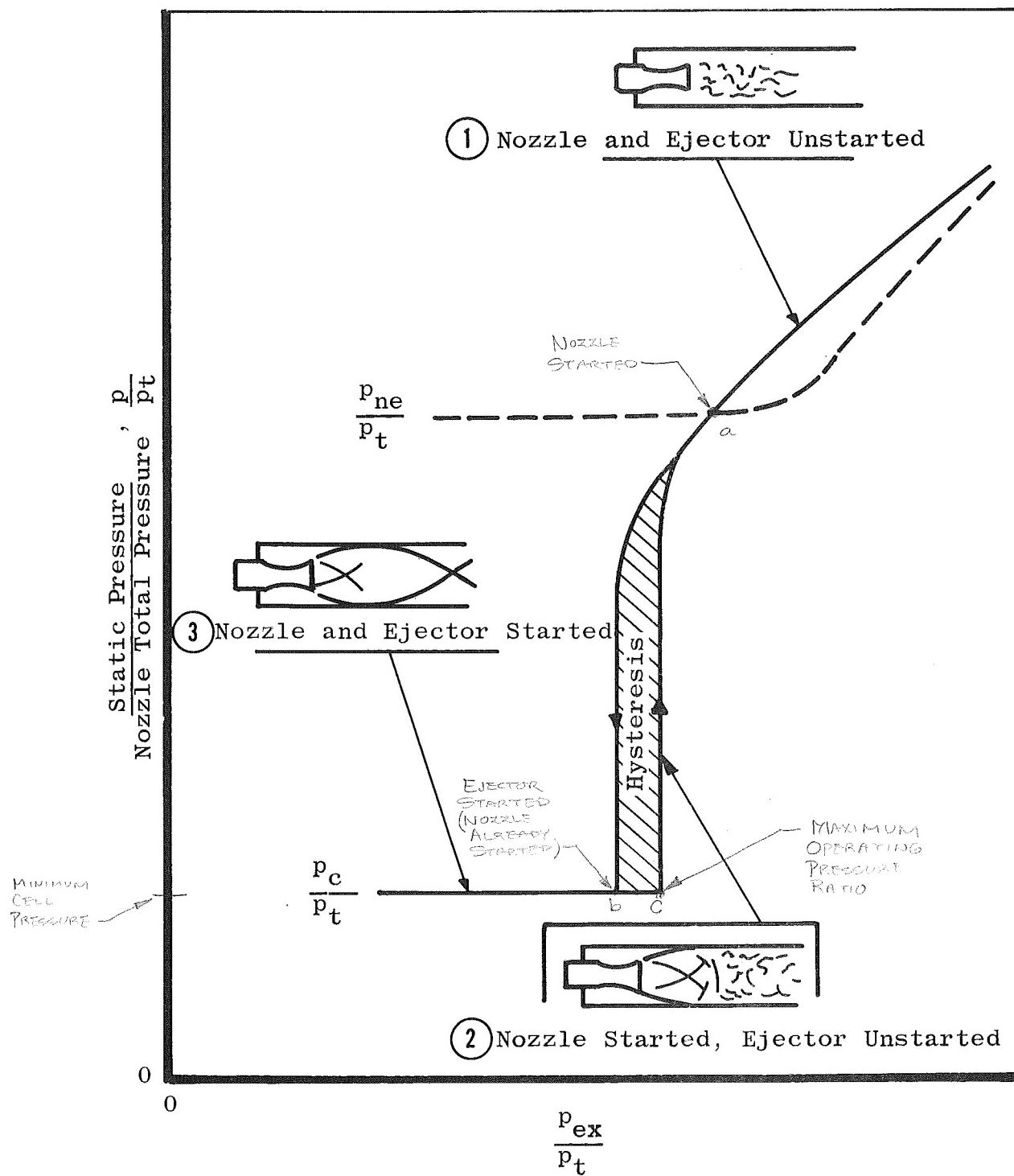
Fig. 1 Typical Ejector System Starting Phenomena for Constant Nozzle Total Pressure

The figure contains the following equations and labels:

$$\frac{\Sigma F}{\dot{m}\sqrt{RT_t}} = \sqrt{\frac{2\gamma}{\gamma - 1}}\frac{2C_f\left(\frac{L}{D}\right)}{\left(M_3 - M_2\right)}$$

$$X\left[\sqrt{\frac{2}{\gamma - 1} + M_3^2} - \sqrt{\frac{2}{\gamma - 1} + M_2^2}\right]$$

$$+ \frac{1 + \gamma M_3^2}{M_3\sqrt{\gamma\left(1 + \frac{\gamma - 1}{2}M_3^2\right)}}$$

$\gamma = 1.4$

$C_f = 0.003$

$\frac{L}{D} = 8.0$

(with Friction)

$\gamma = 1.1$
1.2
1.3
1.4

(without Friction)

$$\frac{\Sigma F}{\dot{m}\sqrt{RT_t}} = \frac{1 + \gamma M_3^2}{M_3\sqrt{\gamma\left(1 + \frac{\gamma - 1}{2}M_3^2\right)}}$$

Vertical axis: $\frac{\Sigma F}{\dot{m}\sqrt{RT_t}}$

Horizontal axis: M_3
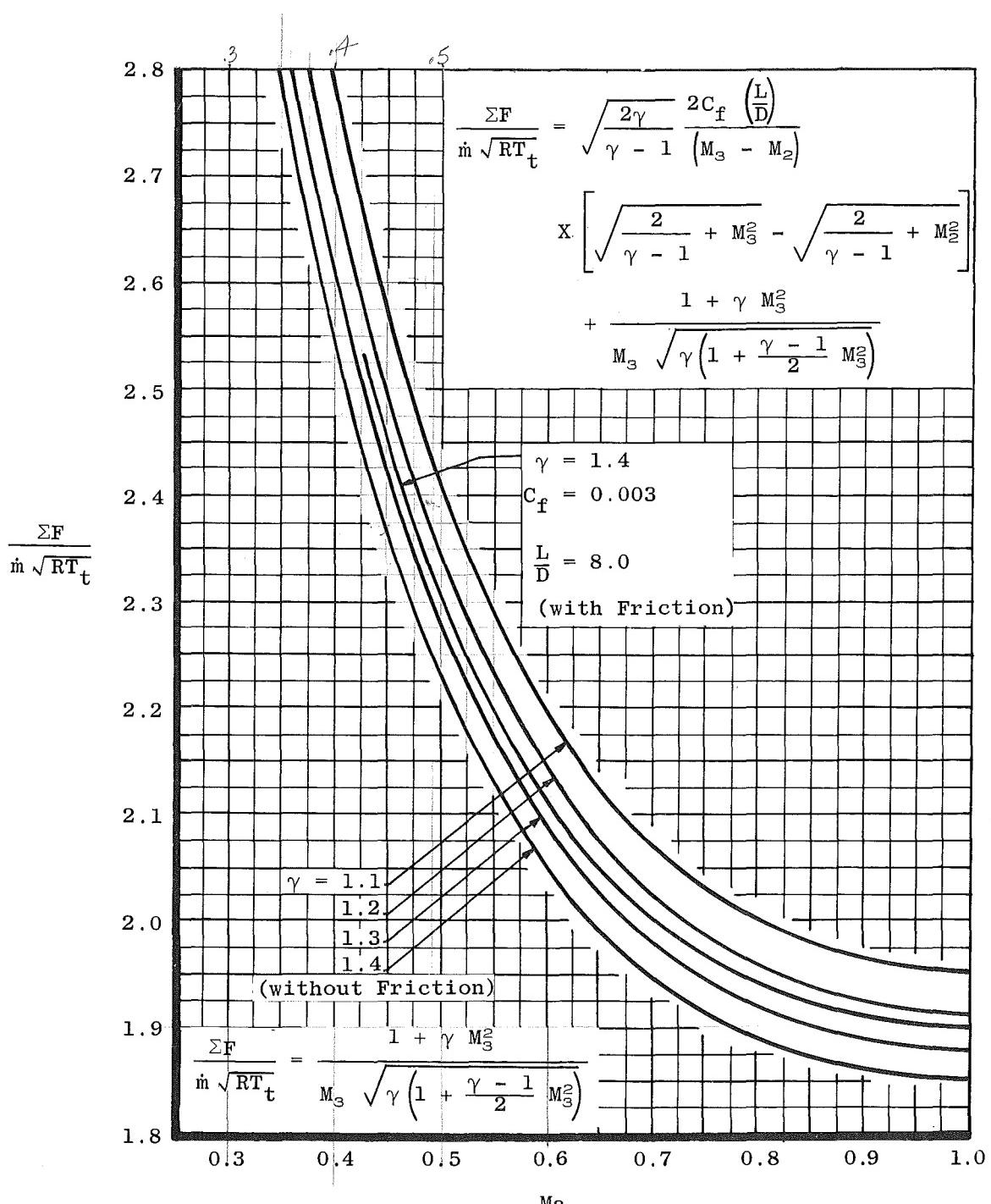
a. Subsonic Solution

Fig. 2 Graphical Solution for Mach Number

$$\frac{\Sigma F}{\dot{m}\sqrt{RT_t}} = \frac{1 + \gamma\, M_2^2}{M_2\sqrt{\gamma\left(1 + \dfrac{\gamma - 1}{2}\, M_2^2\right)}}$$
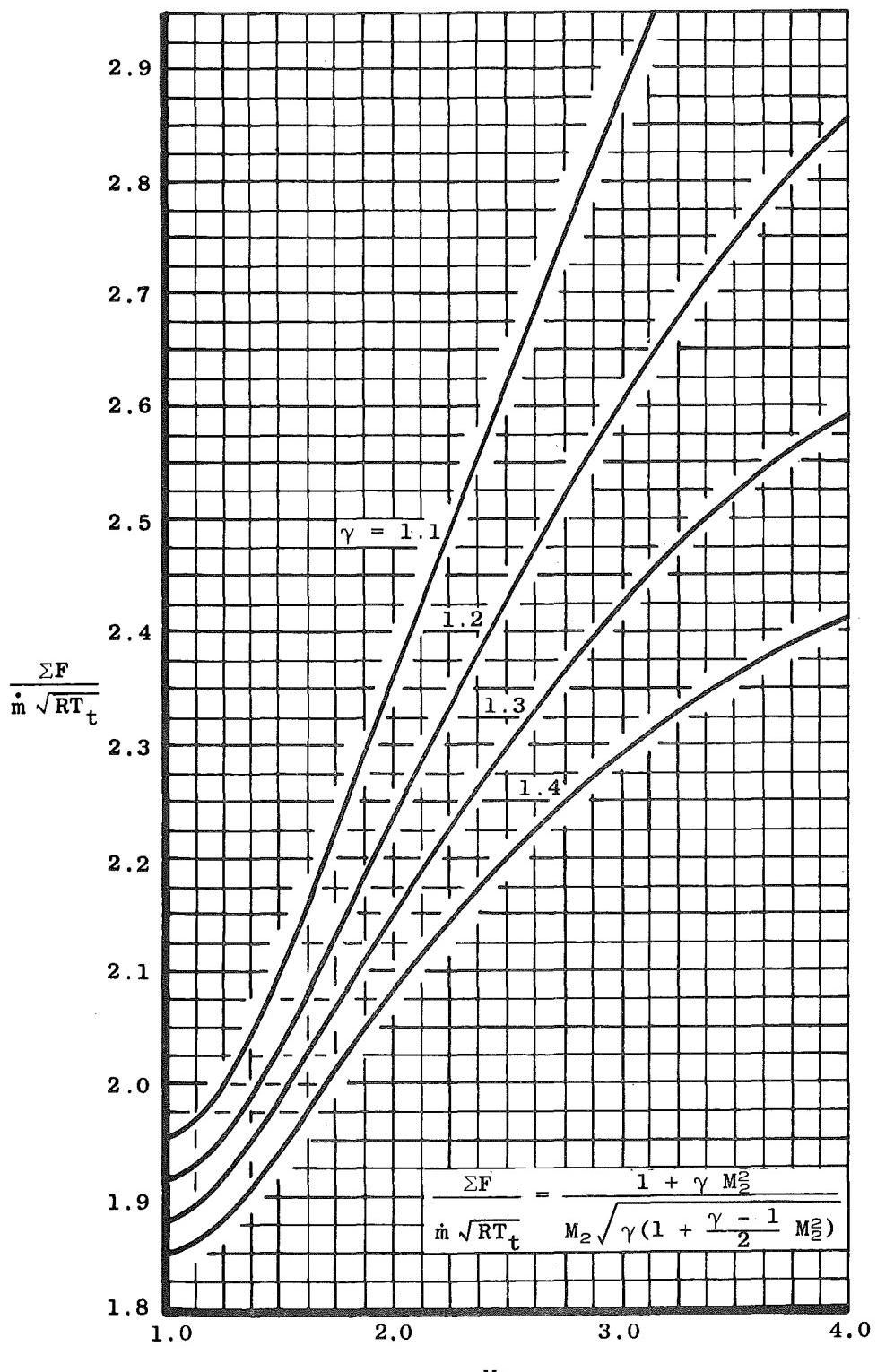
b. Supersonic Solution

Fig. 2 Concluded
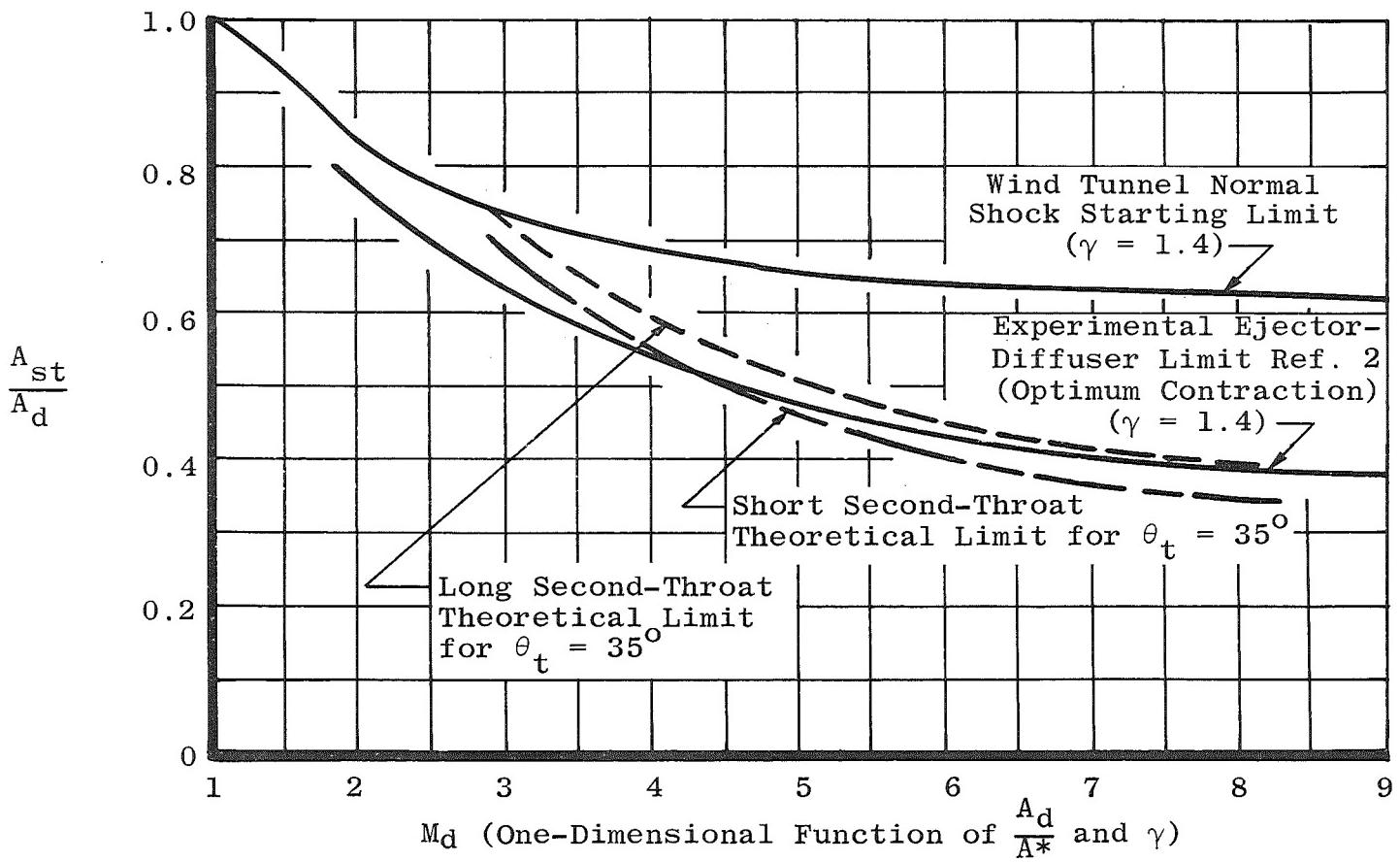
Fig. 3 Comparison of Second-Throat Starting Limits

Wall Static Pressure Taps

Telescoping Section

T_t

Inlet

30 in. diam

p_c

p_t

x_{st}

D_{st}

Exhaust

θ_{st}

L_{st}

3-in. Gate Valve

Actuating Mechanism of Movable Nozzle System

Sealed Plenum Chamber
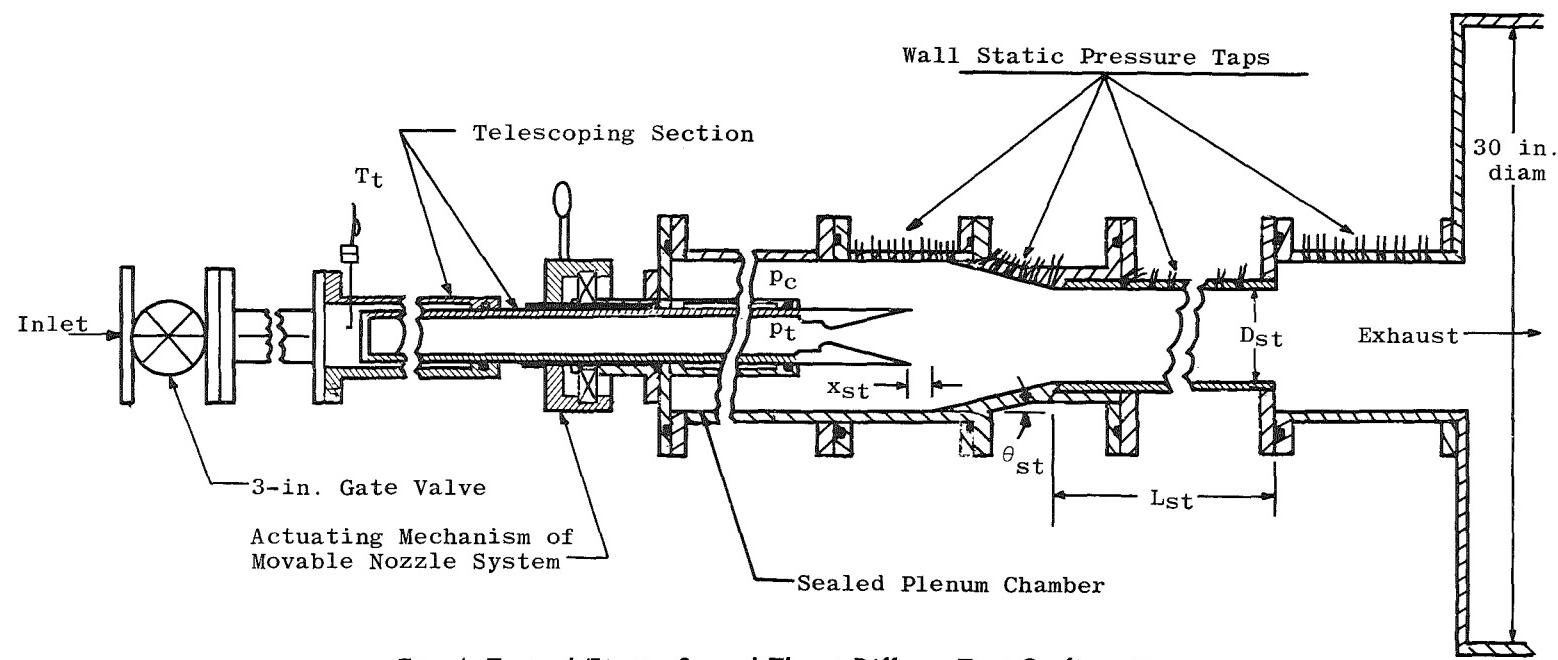
Fig. 4 Typical Ejector Second-Throat Diffuser Test Configuration

The figure shows a graph with:

- Vertical axis: $\frac{A_{st}}{A_d}$ ranging from 0 to 1.0
- Horizontal axis: M_d (One-Dimensional Function of $\frac{A_d}{A^*}$ and γ) ranging from 1 to 9

Legend at top:
Open Symbols — Ejector Started
Closed Symbols — Ejector would not Start
Flagged Symbols — $(L/D)_{st} \approx 8.0$
Unflagged Symbols — $(L/D)_{st} < 1$

Labels on curves:
Wind Tunnel Normal Shock Starting Limit $(\gamma = 1.4)$

Experimental Ejector-Diffuser Limit Ref. 2 (Optimum Contraction) $(\gamma = 1.4)$

Sym	Nozzle	A_{ne}/A^*	θ_{ne}
O	1	3.63	18°
□	3	10.85	18°
△	4	25.00	18°
◇	5	23.68	0°
◠	8	18.57	18°

Fig. 5 Comparison of Experimental Second-Throat Starting Performance with the Empirical Starting Limit
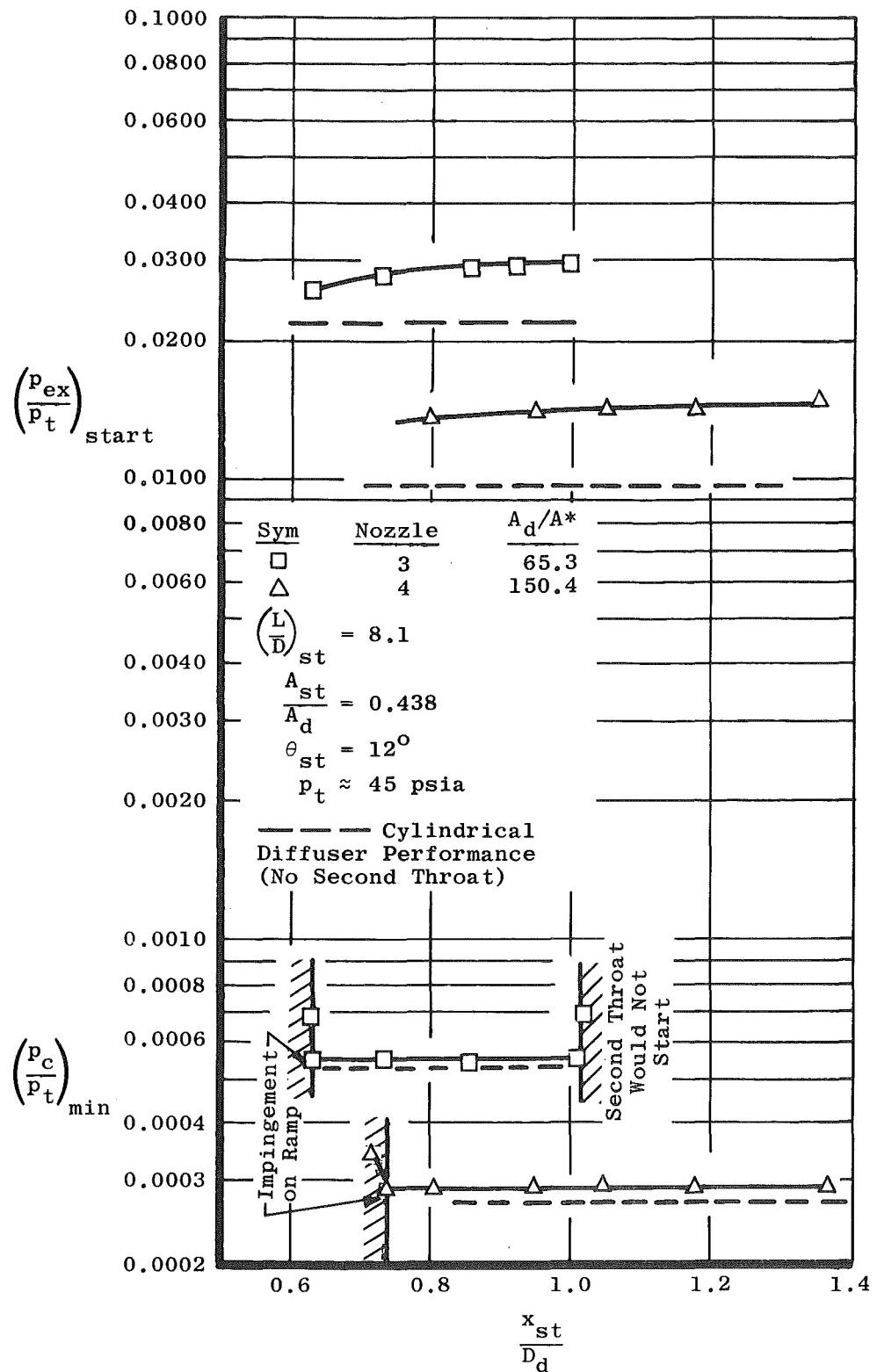
Fig. 6 Ejector-Diffuser Performance for Various Second-Throat Positions
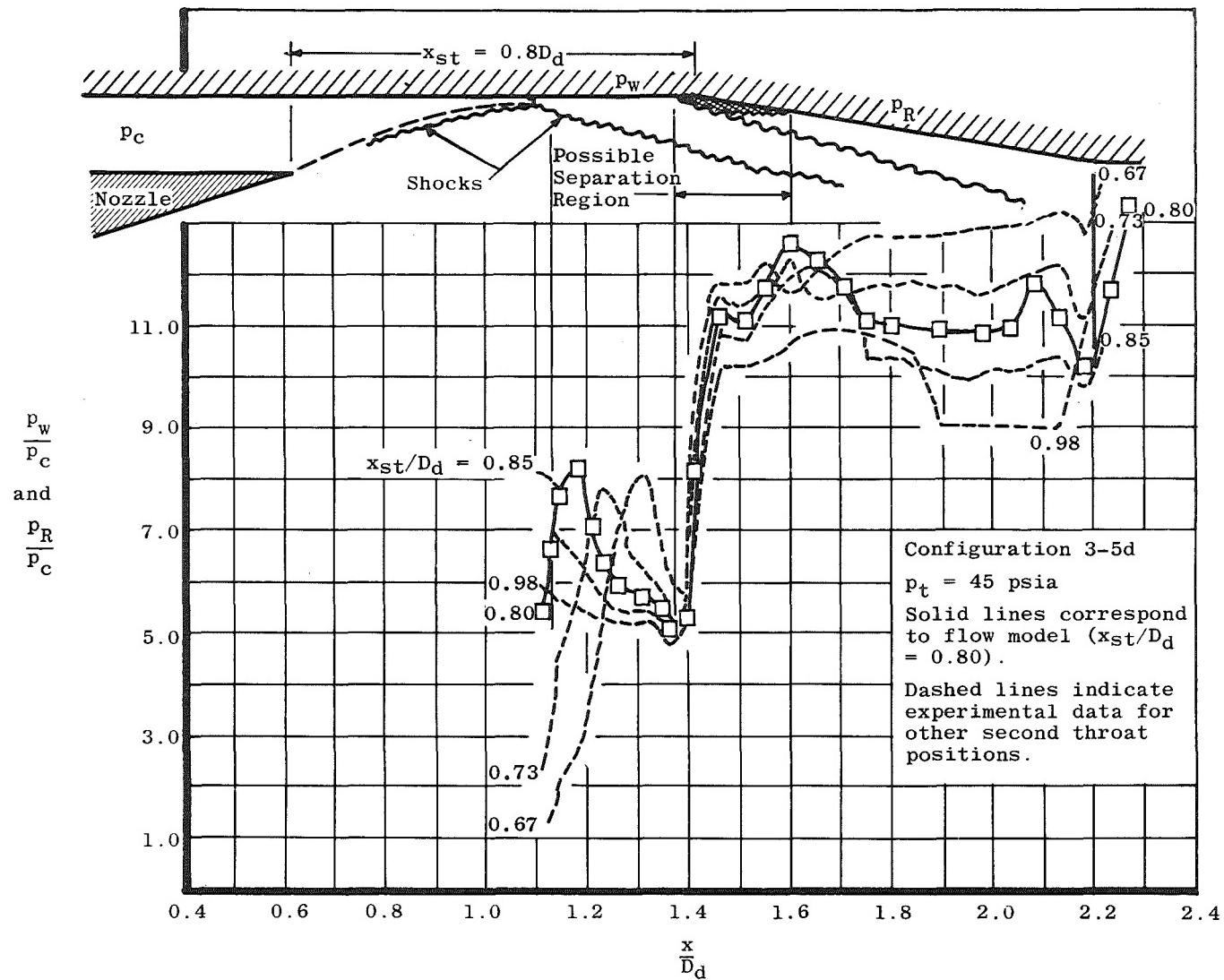
Fig. 7 Experimental Static Pressure Distribution along Cylindrical Diffuser and Second-Throat Ramp for Various Second-Throat Positions
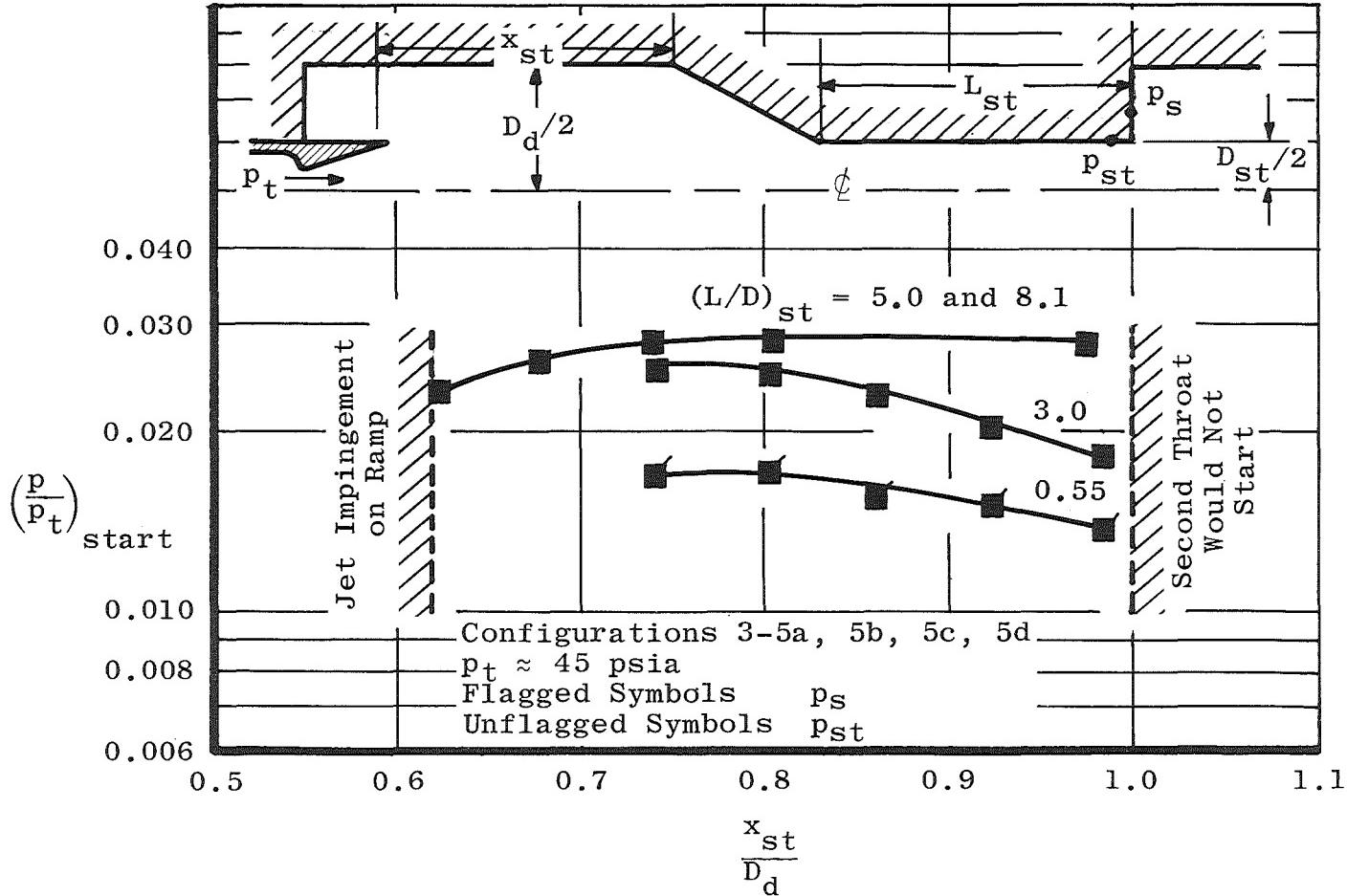
Fig. 8 Variation of Ejector Starting Pressure Ratio with Second-Throat Positions for Various Throat Lengths
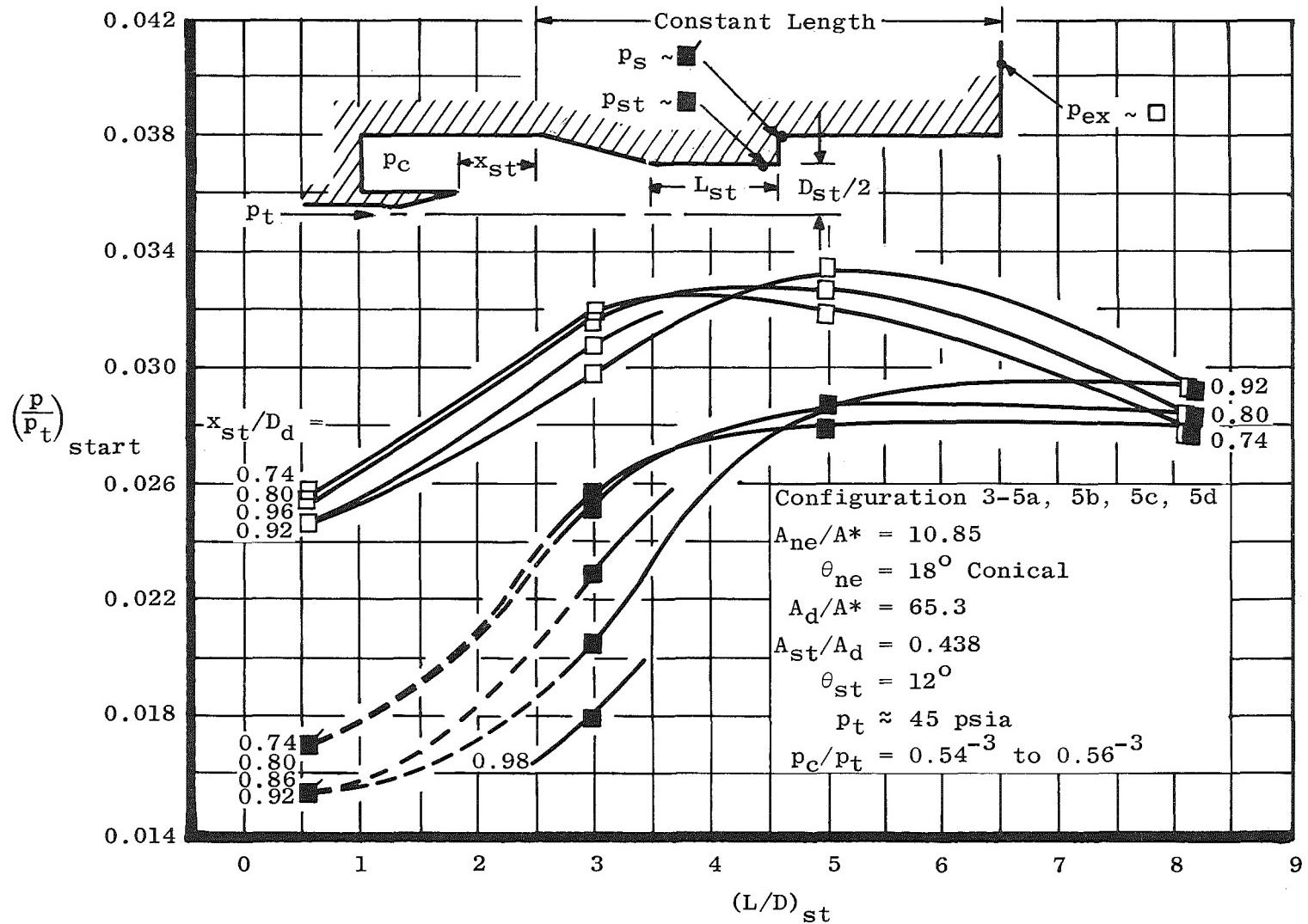
Fig. 9 Effect of Second-Throat Length on Ejector Starting Pressure Ratio for Various Second-Throat Positions
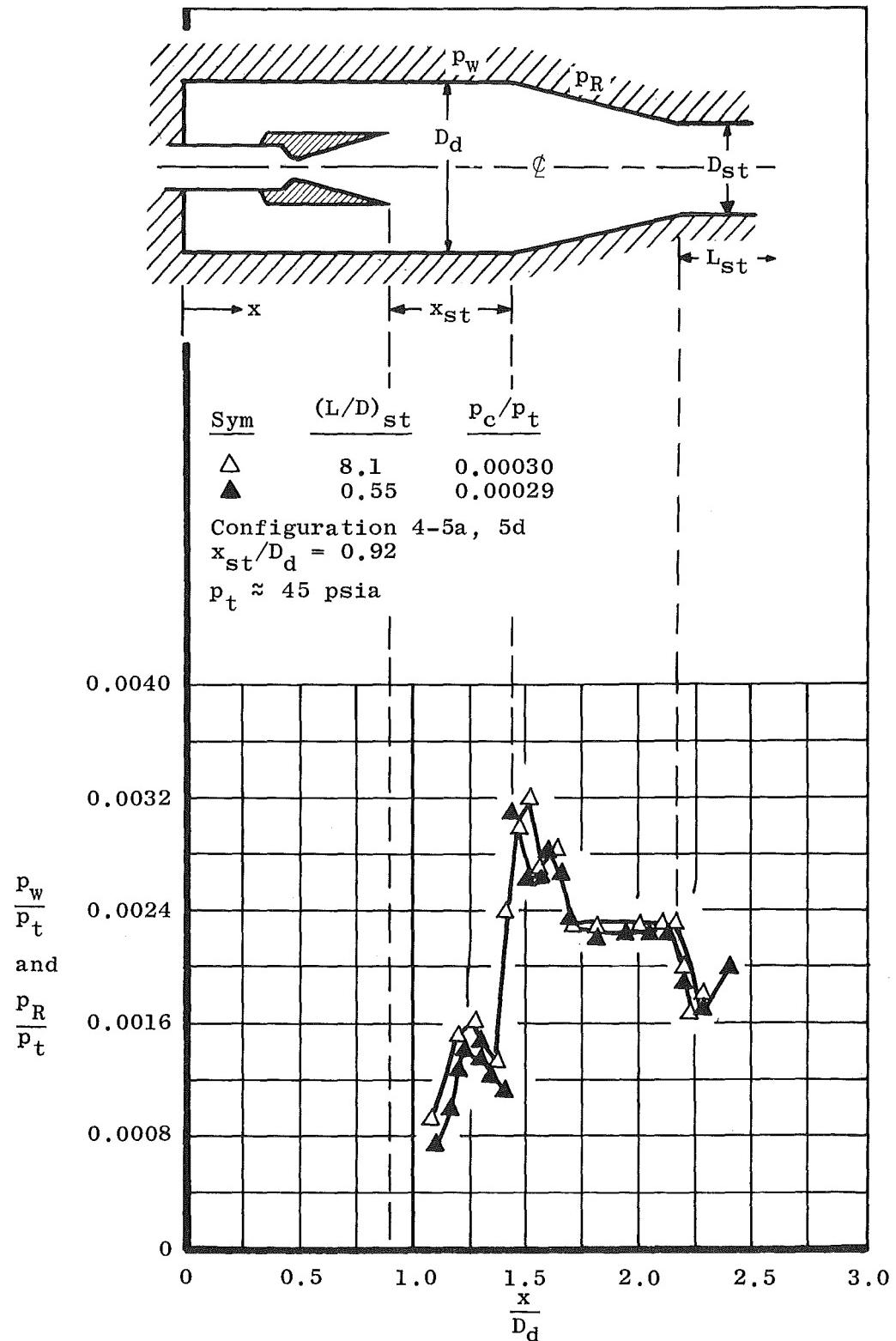
Fig. 10 Wall Static Pressure Distribution Comparison for Long and Short
Second-Throat Lengths

37
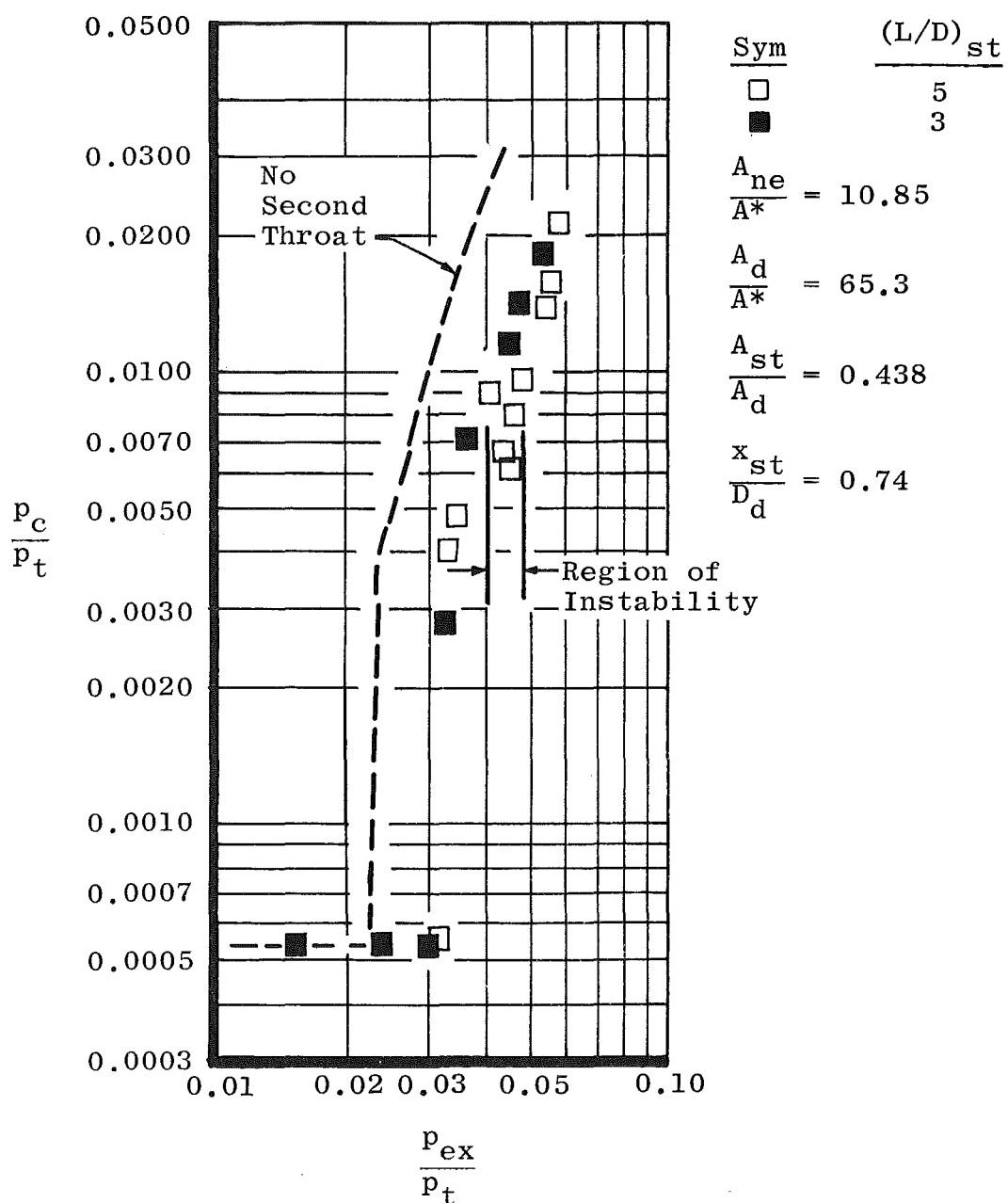
Fig. 11 Ejector-Diffuser Instability

$$\theta_m = \tan^{-1}\left(\frac{r_m}{x_n + x_{st} + x_m}\right)$$

$$\theta_t = \theta_{st} + \theta_m$$
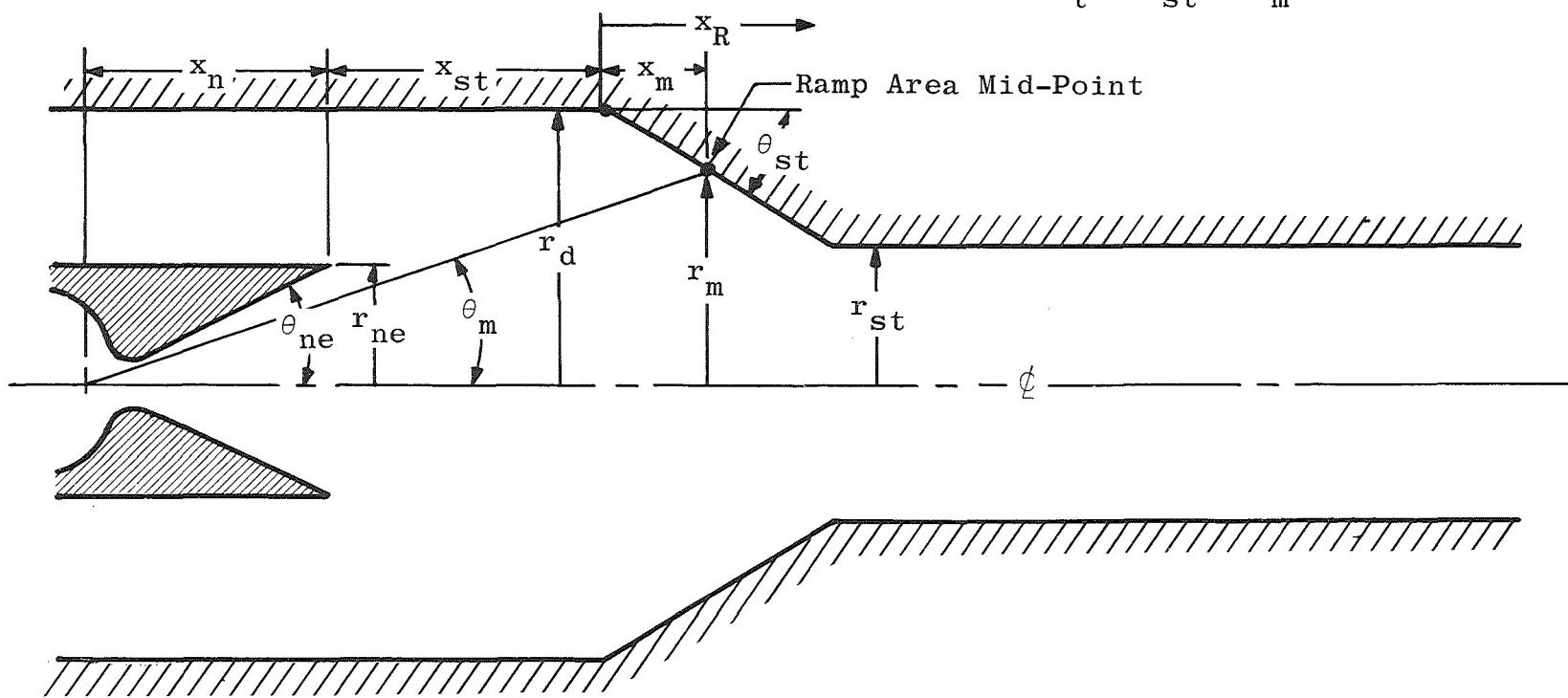
Fig. 12 Schematic of the Geometry for the Mean Gas Expansion Angle Equation
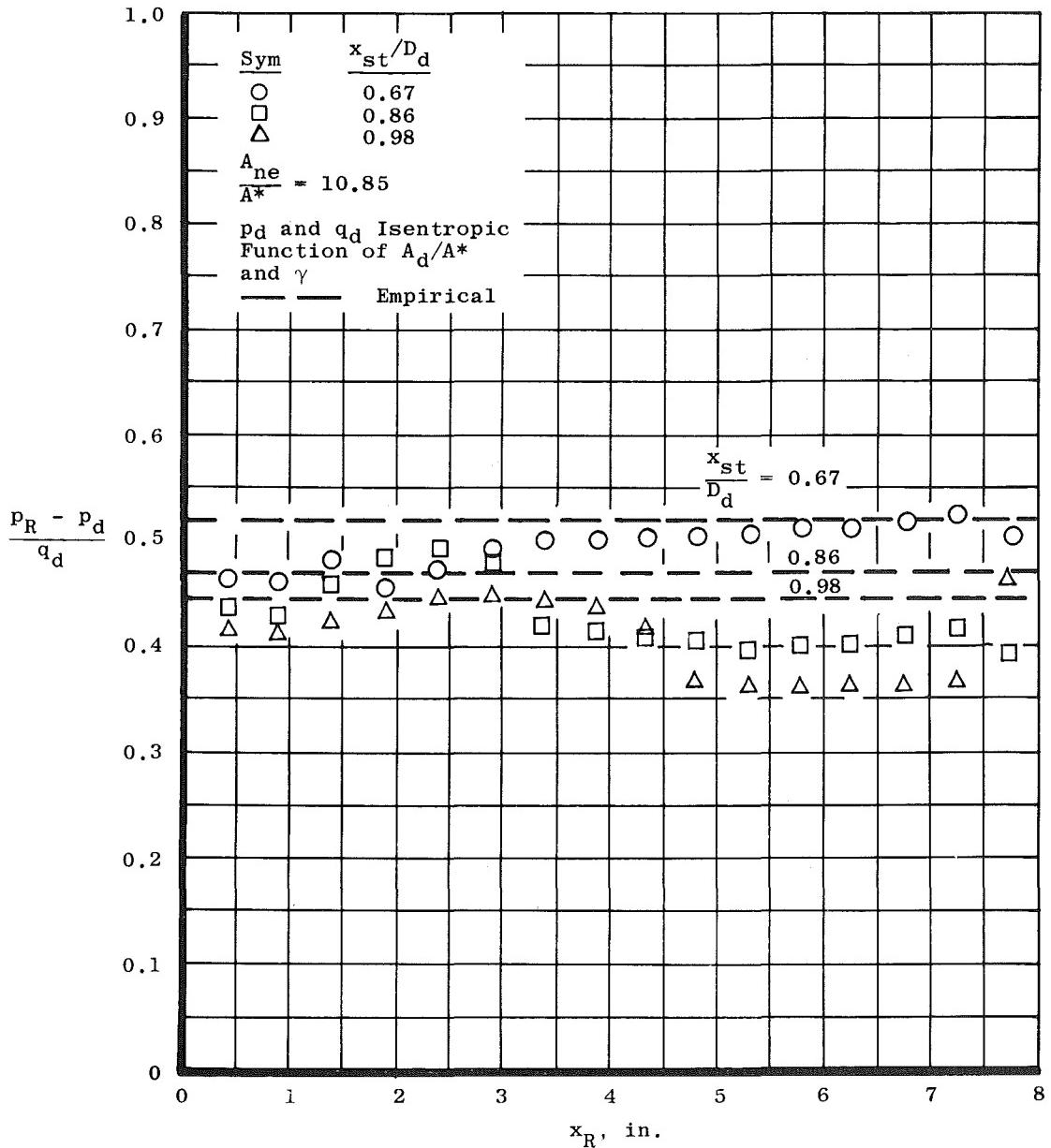
a. Configurations 3-5a and 3-5d

Fig. 13 Comparison of Experimental and Empirical Ramp Pressure Coefficients
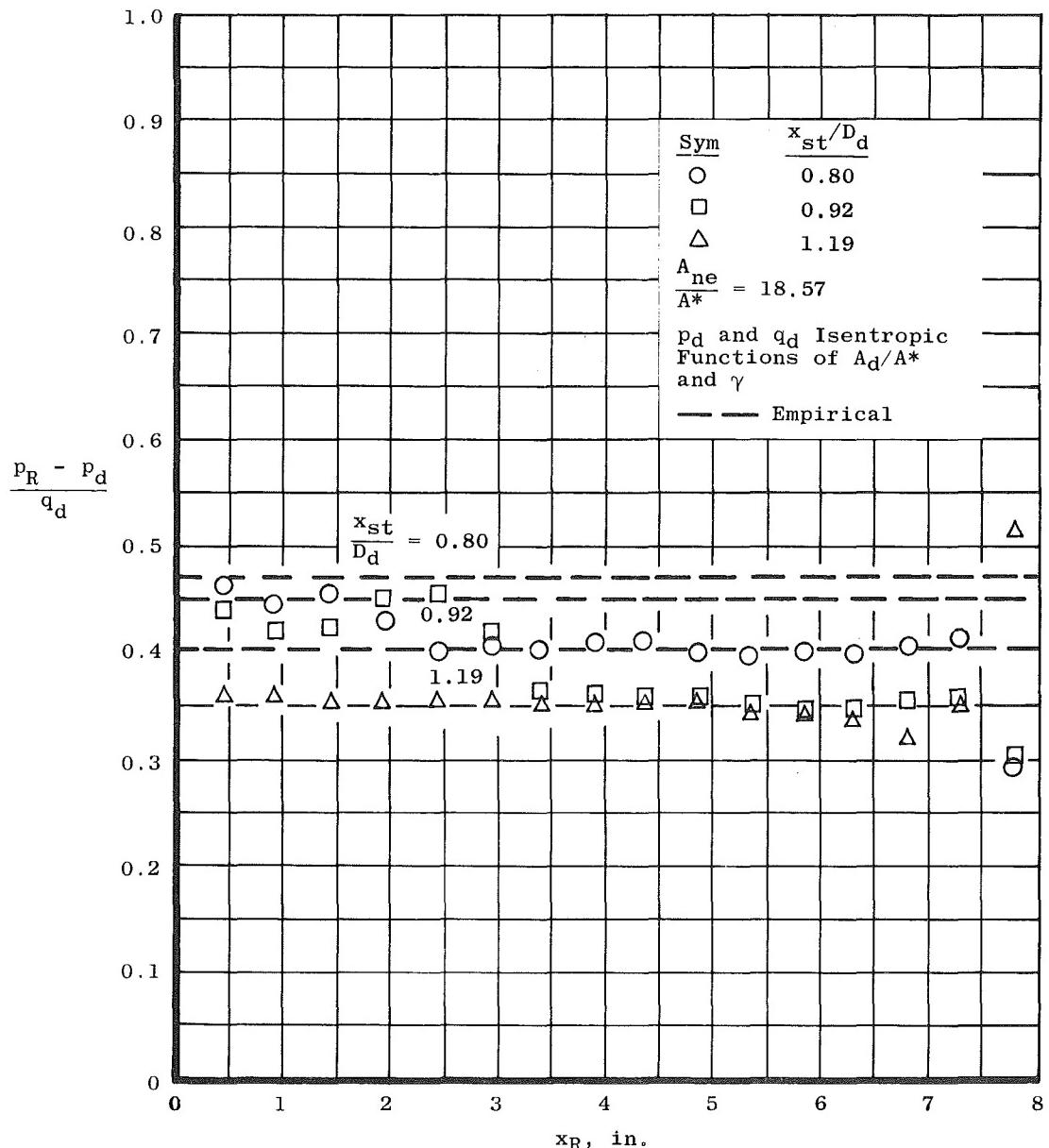
b. Configurations 8-5a and 8-5d

Fig. 13 Continued
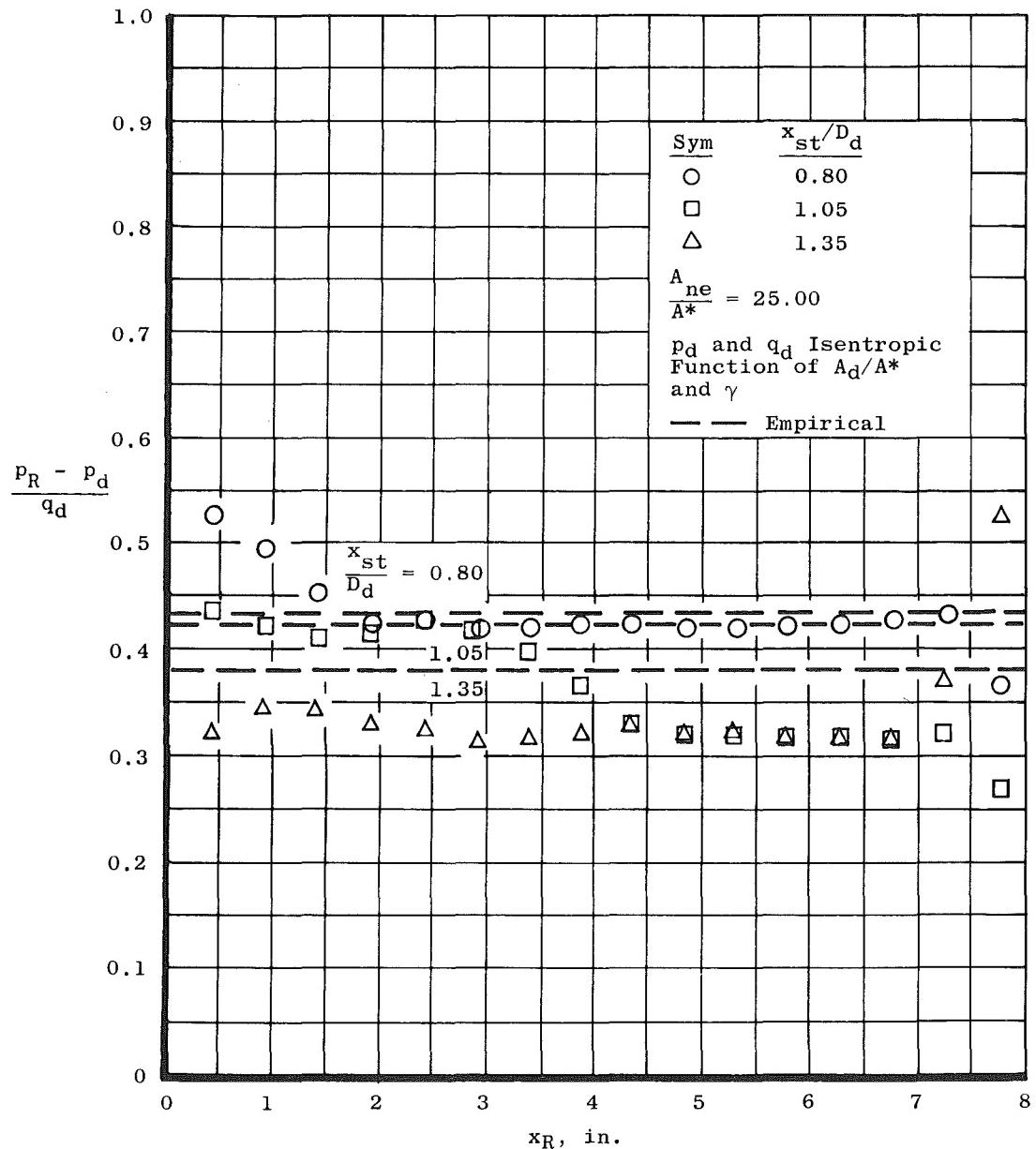
c. Configurations 4-5a and 4-5d

Fig. 13 Concluded
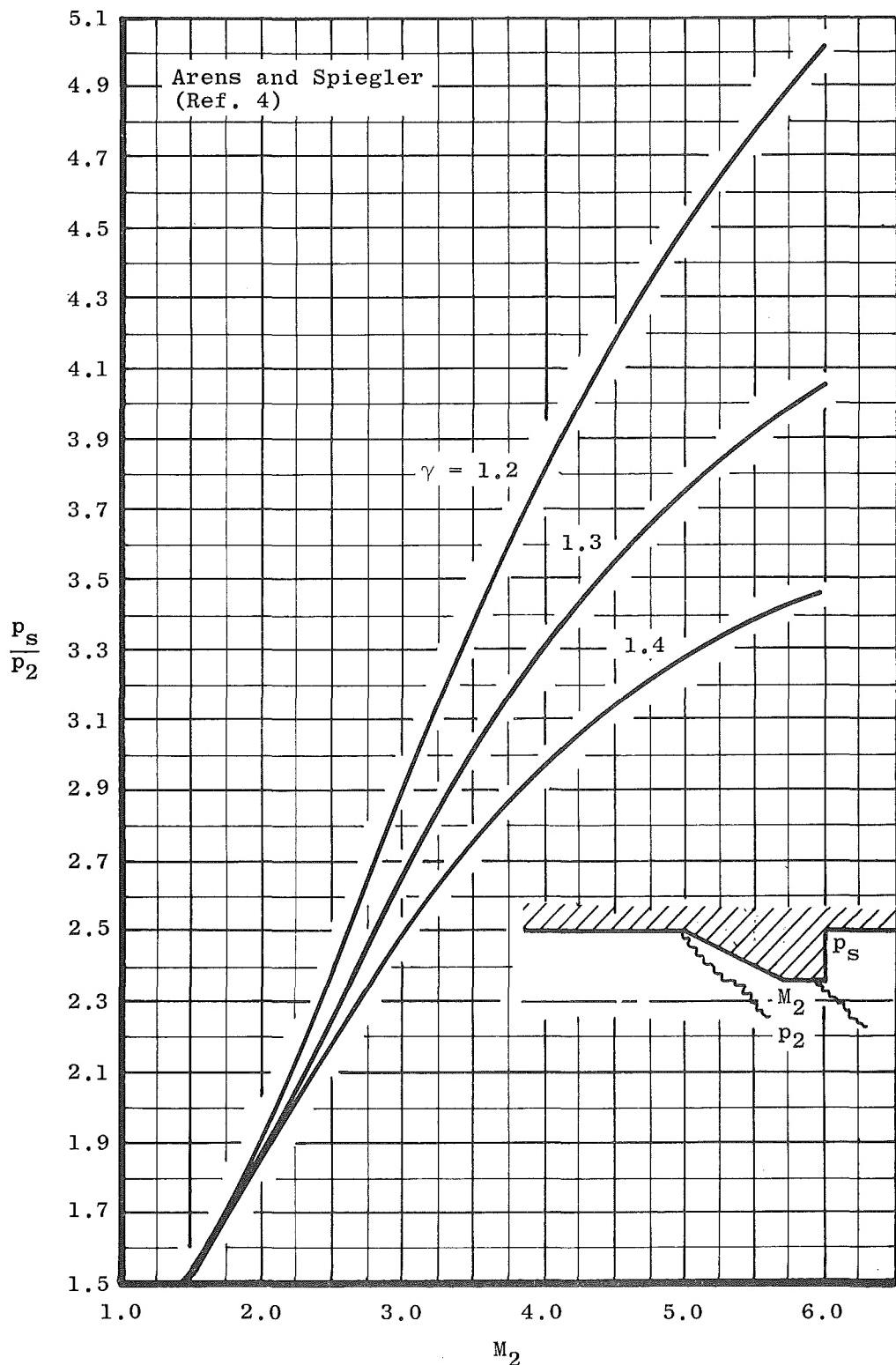
Fig. 14 Free, Shock-Separation Pressure Ratio
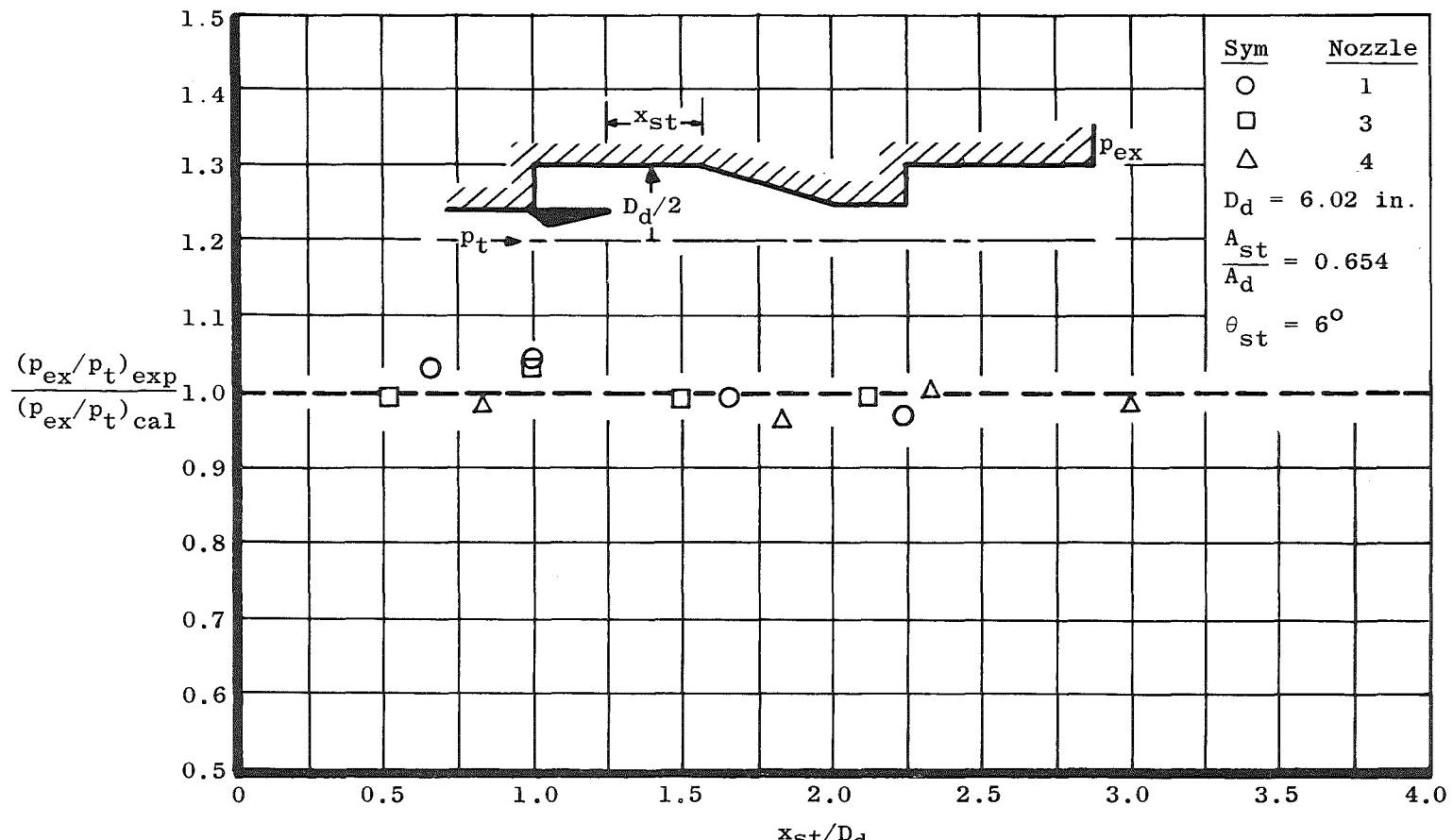
a. Configurations 1-1a, 3-1a and 4-1a

Fig. 15 Comparison of Calculated Starting Pressure Ratio with Experimental Results for Short Second Throats
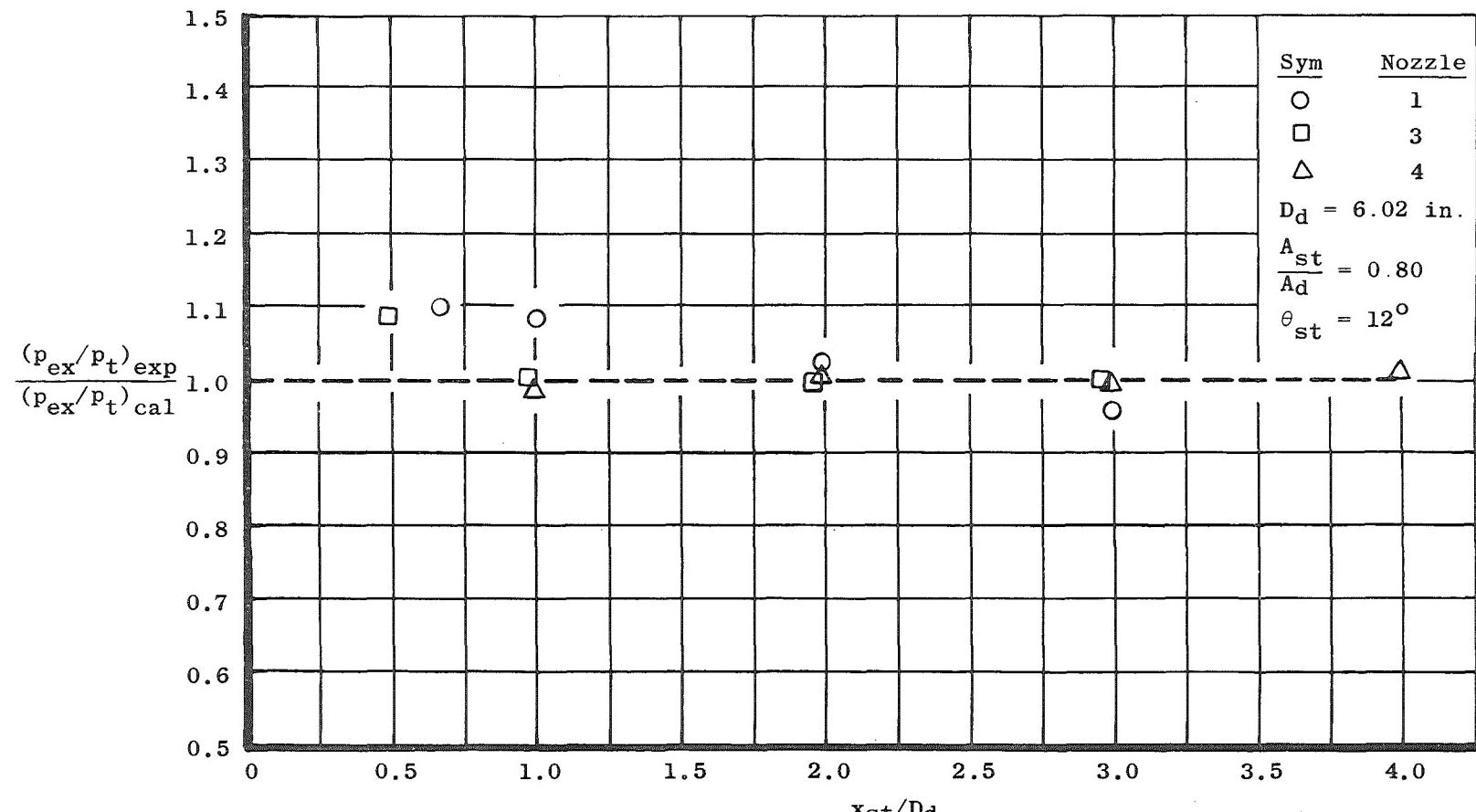
b. Configurations 1-2a, 3-2a and 4-2a

Fig. 15 Continued
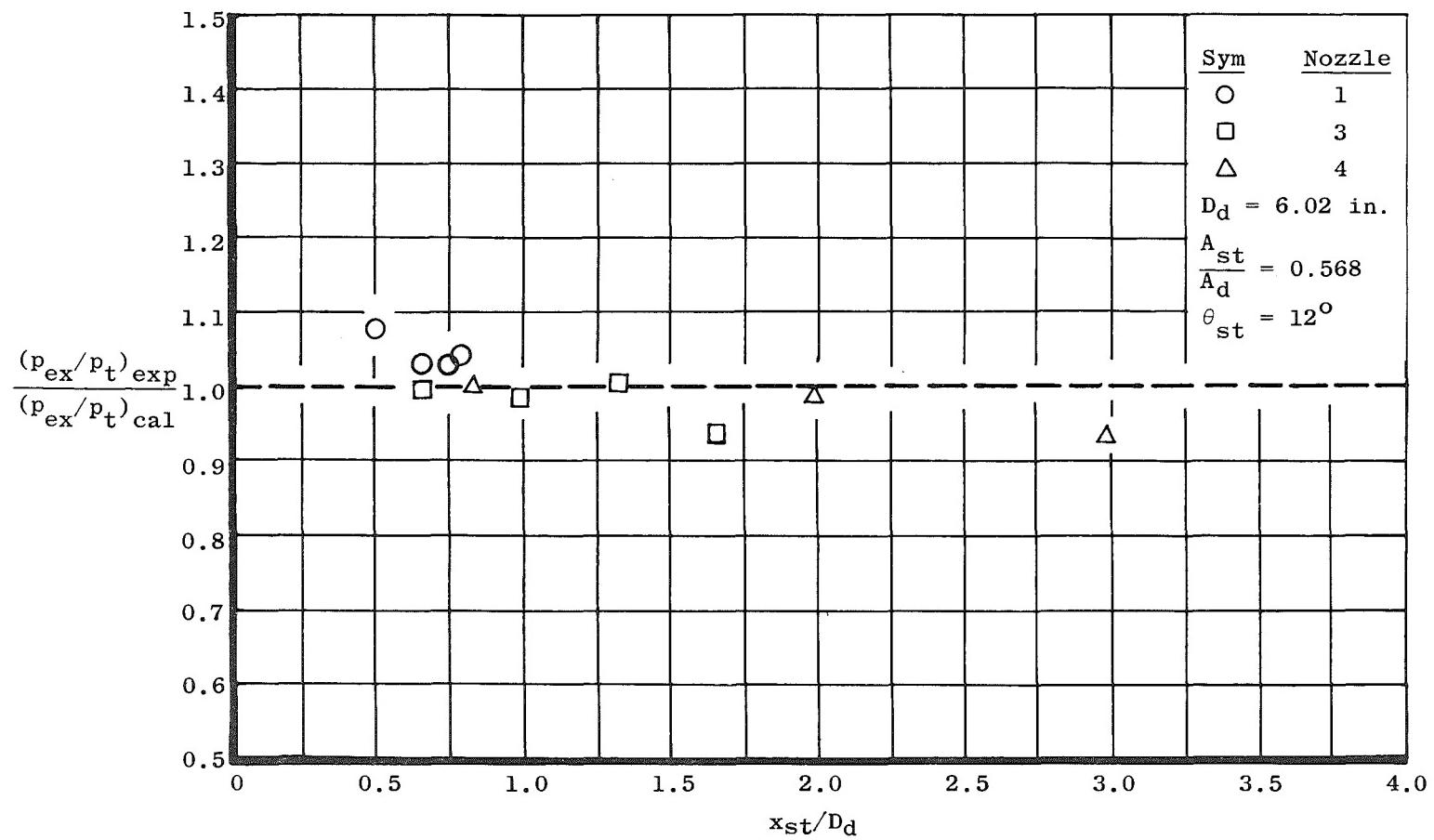
c. Configurations 1-2b, 3-2b and 4-2b

Fig. 15 Continued
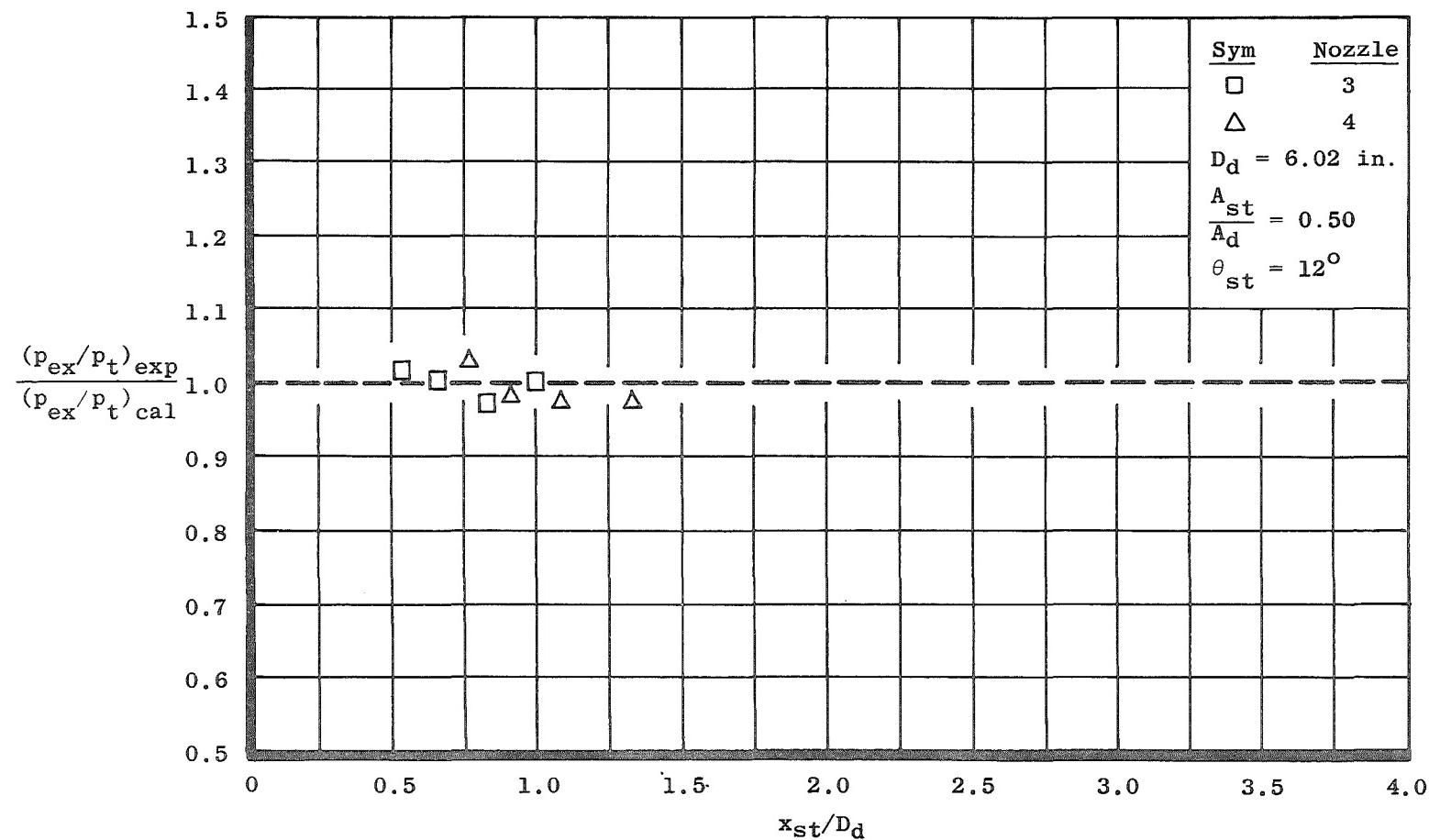
d. Configurations 3-3a and 4-3a

Fig. 15 Continued
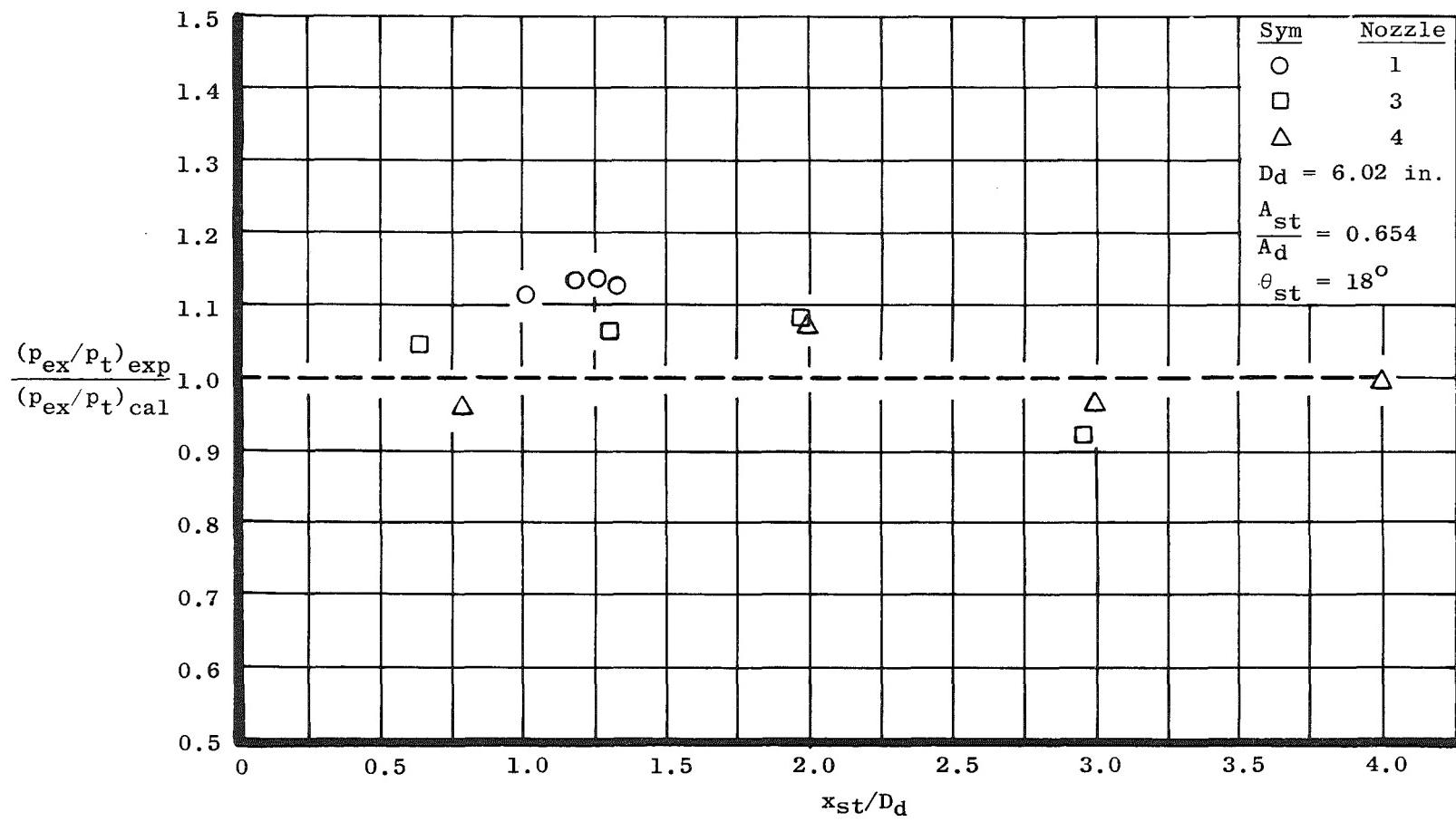
e. Configurations 1-4a, 3-4a and 4-4a

Fig. 15 Continued
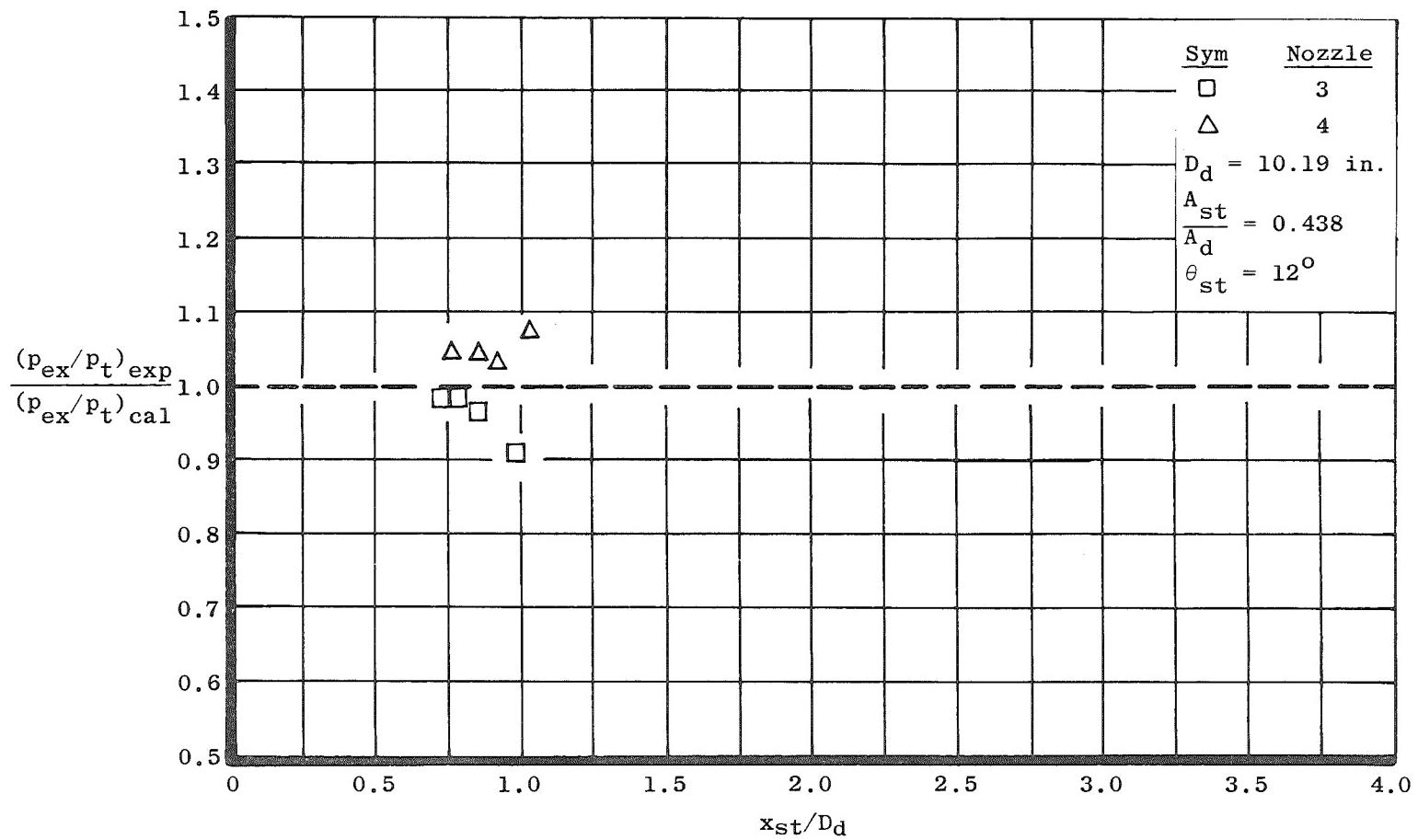
f. Configurations 3-5a and 4-5a

Fig. 15 Concluded
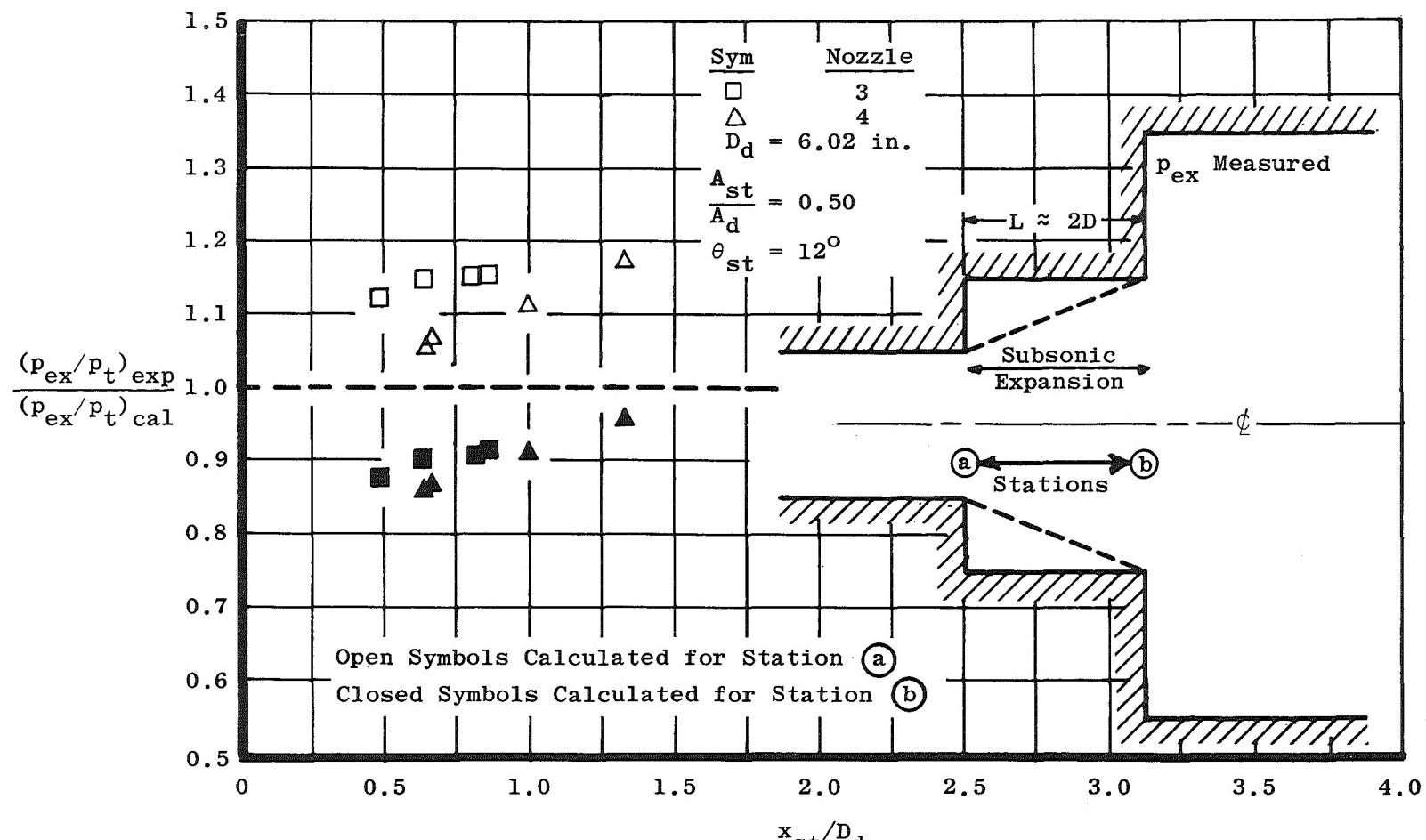
a. Configurations 3-3b and 4-3b

Fig. 16 Comparison of Calculated Starting Pressure Ratios with Experimental Results for Long Second Throats
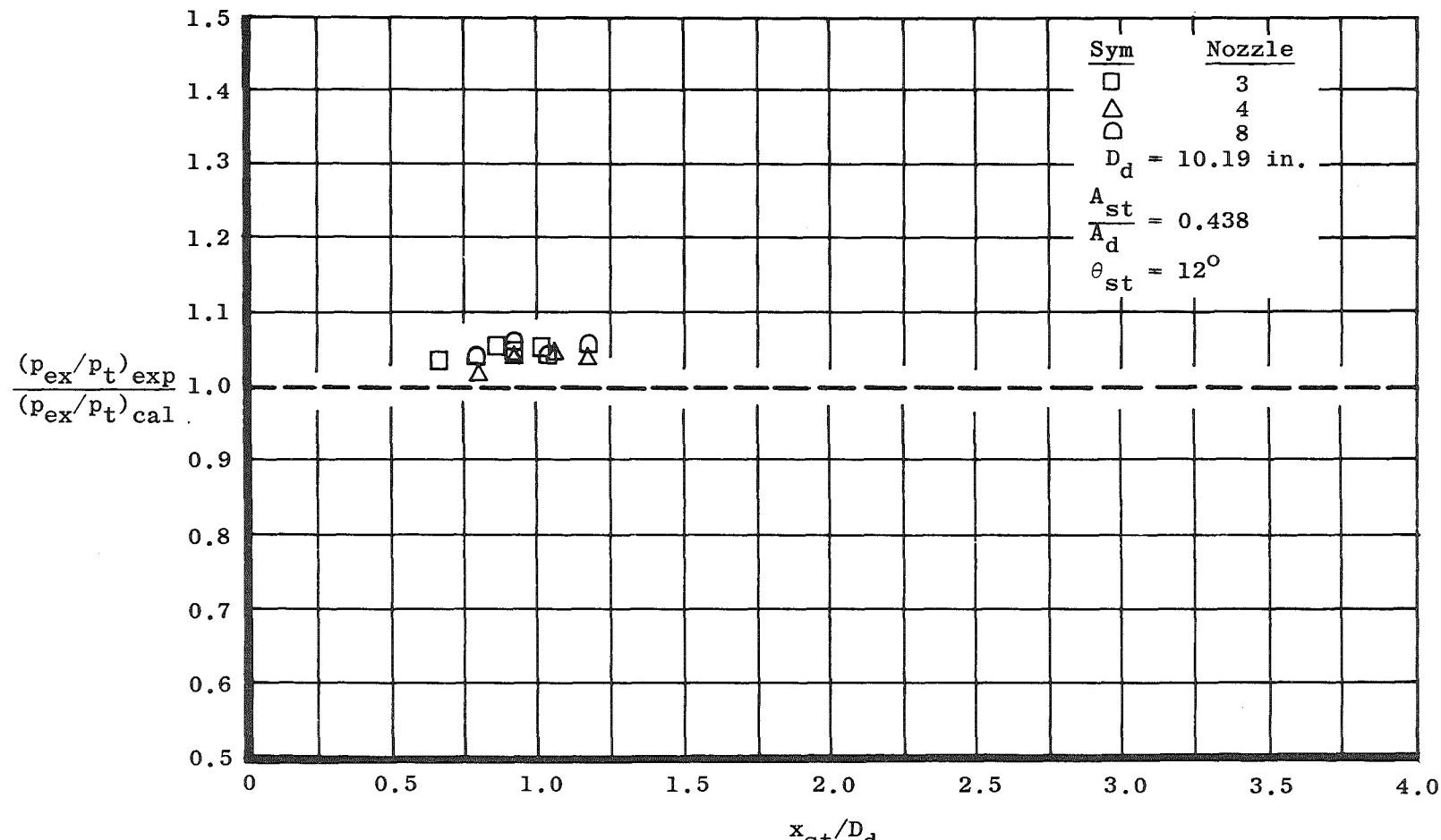
b. Configurations 3-5d, 4-5d and 8-5d

Fig. 16 Concluded

a. $\gamma = 1.3$
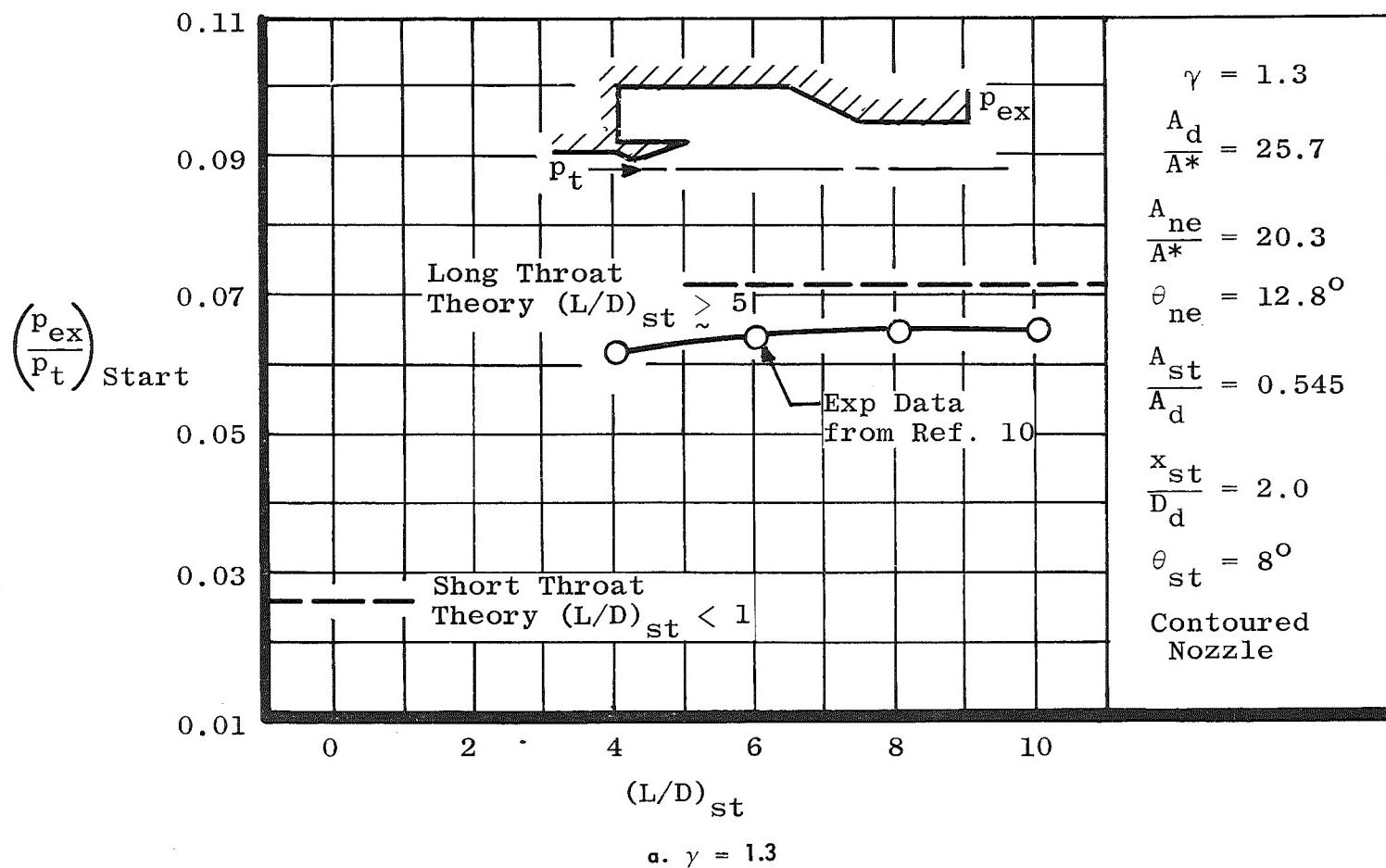
Fig. 17 Comparison of Theoretical and Experimental Ejector Second-Throat Starting Pressure Ratio for Hot Flow
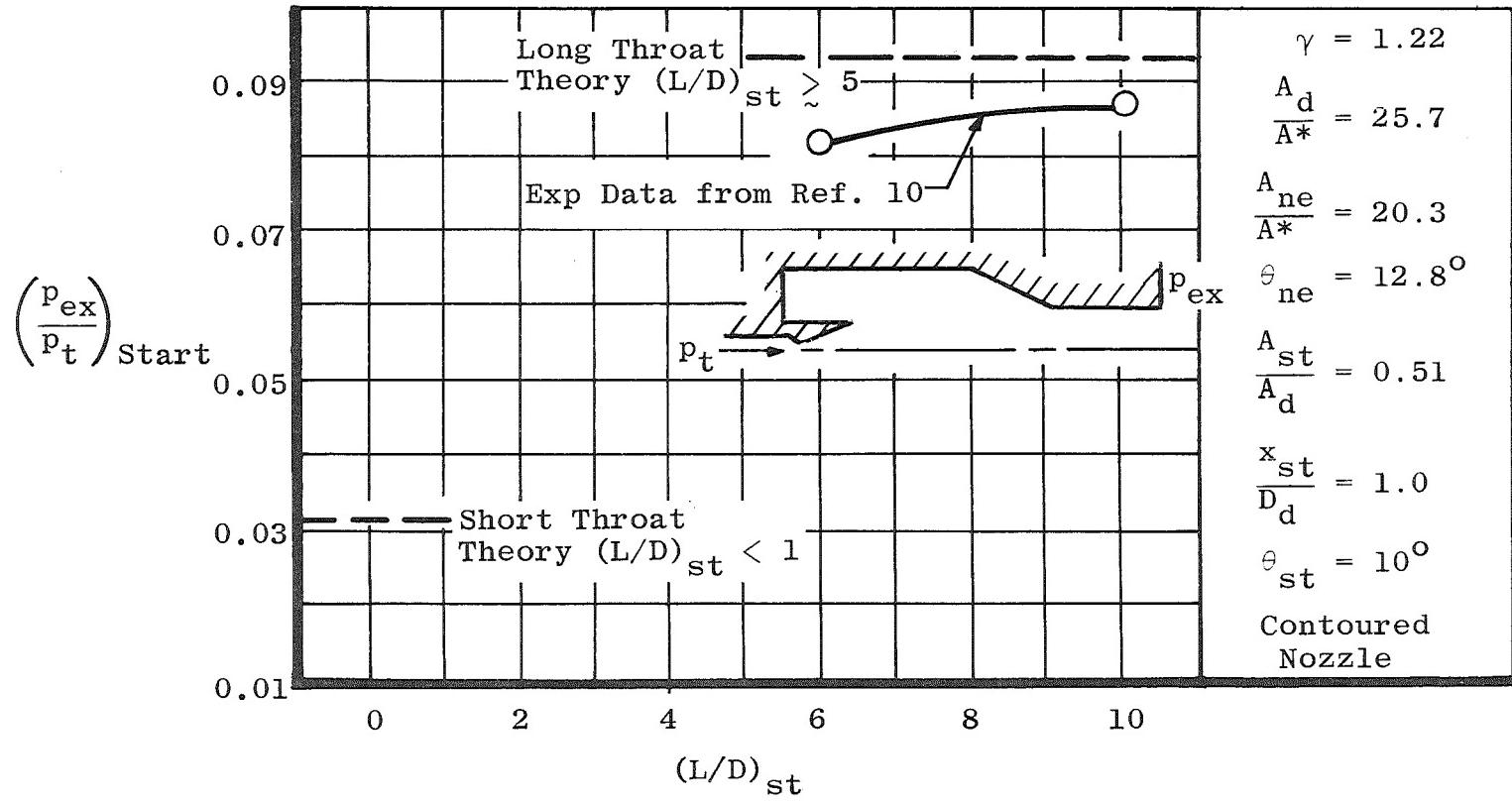
b. $\gamma = 1.22$

Fig. 17 Concluded
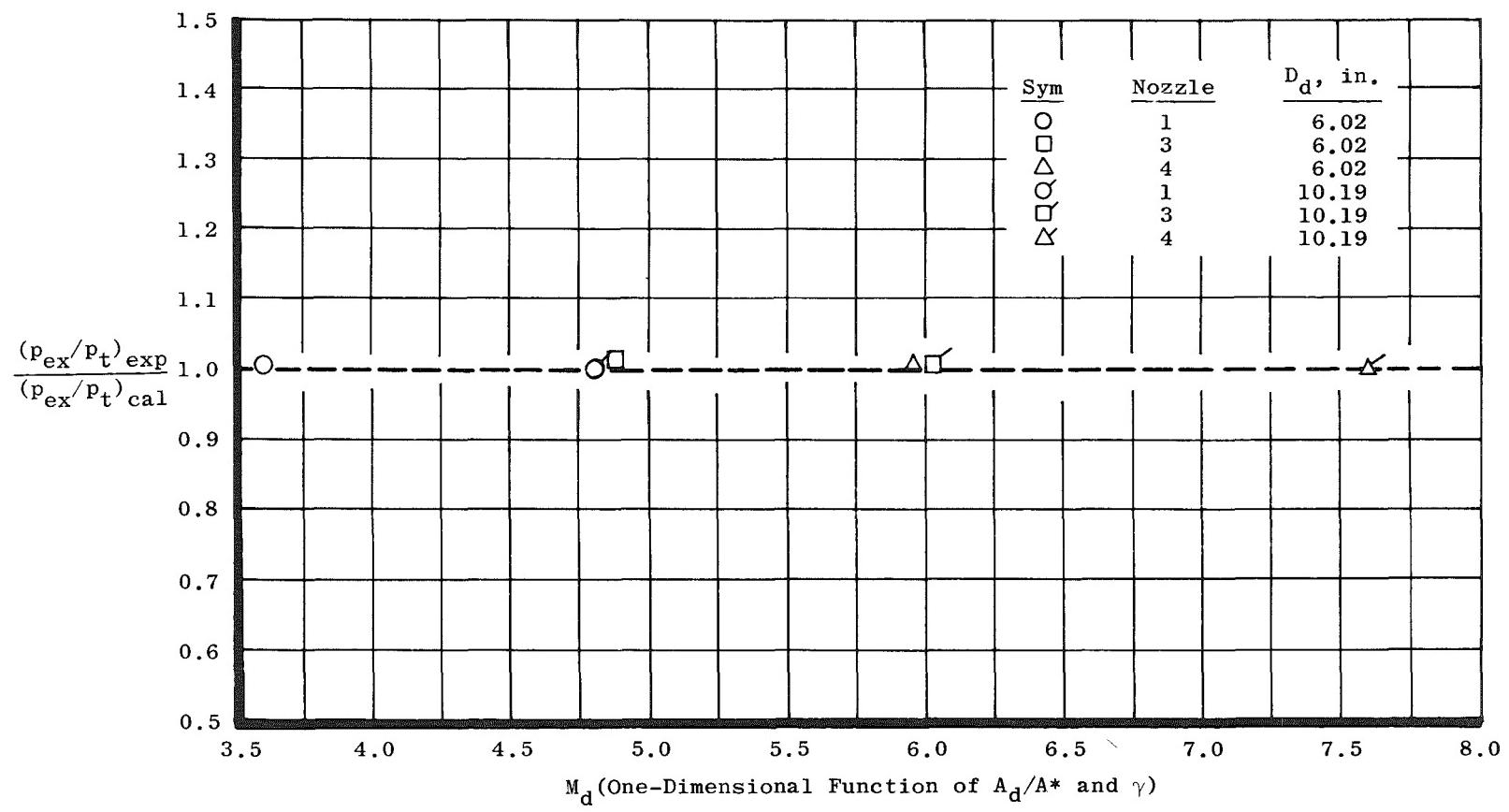
Fig. 18 Comparison of Calculated and Experimental Starting Pressure Ratios for Cylindrical Diffusers, $(L/D)_d \approx 9$
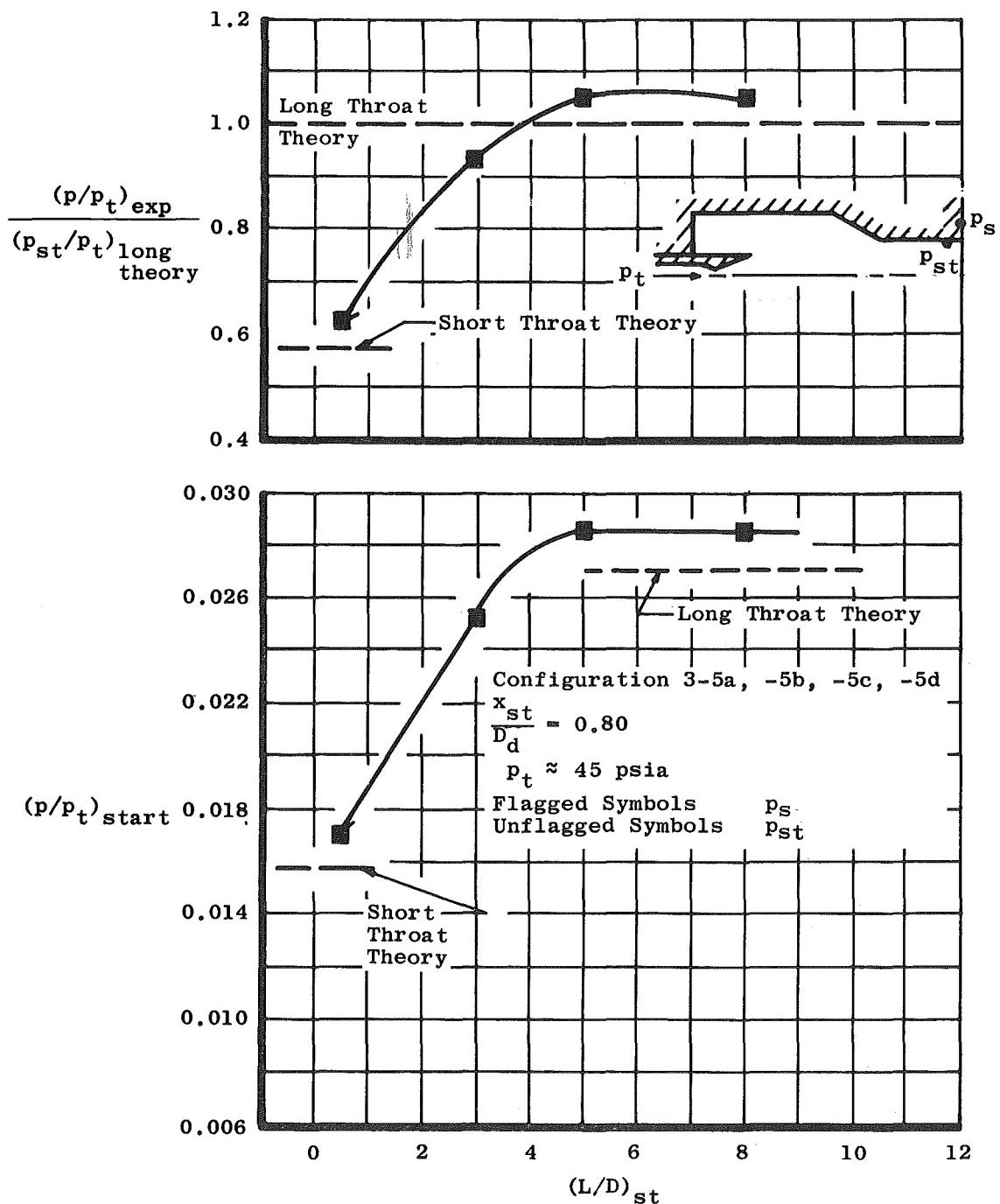
Fig. 19 Comparison of Theoretical and Experimental Starting Pressure Ratios for Various Second-Throat Lengths
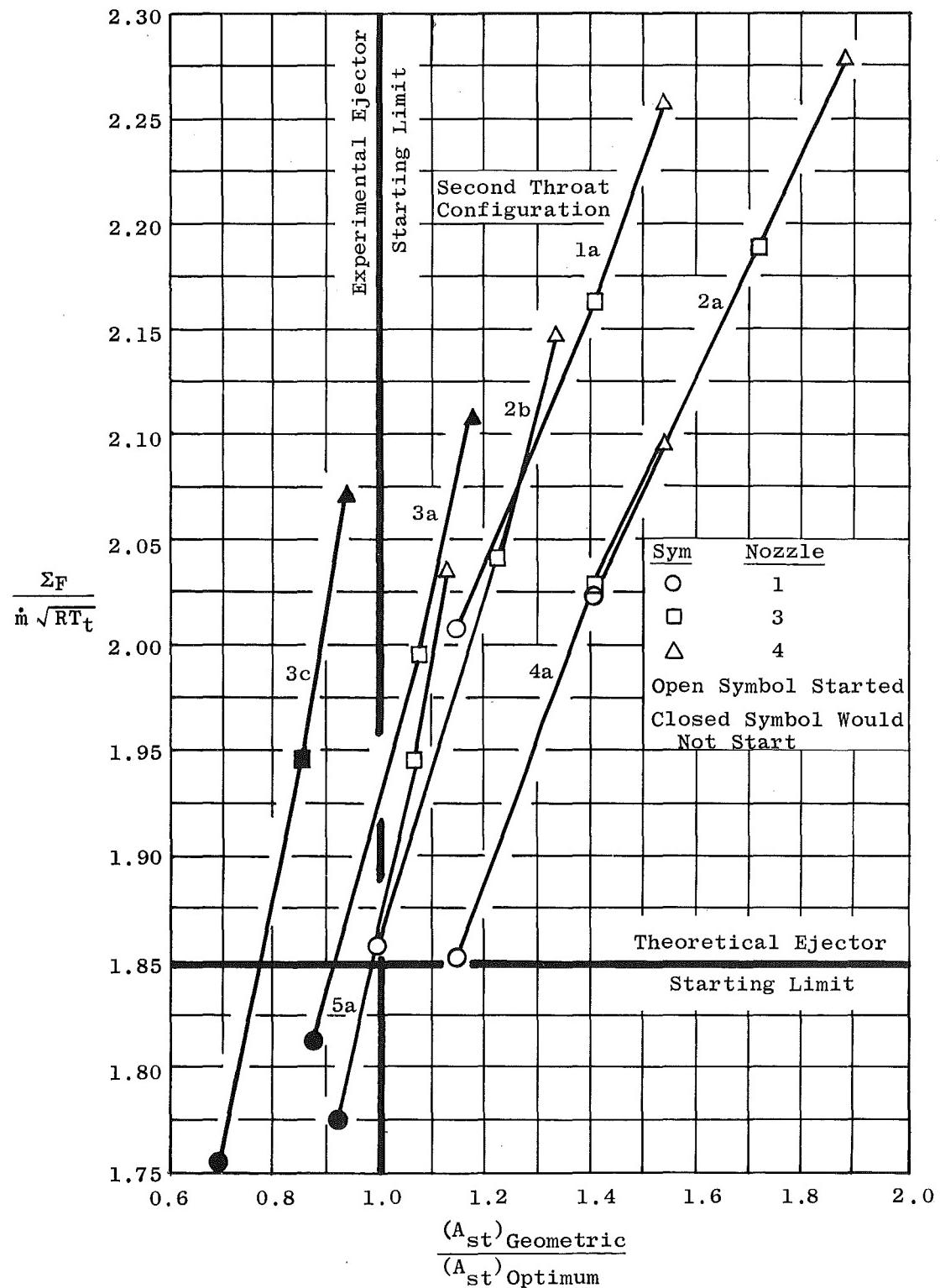
Fig. 20 Comparison of Theoretical and Experimental Short Second-Throat Contraction Limit
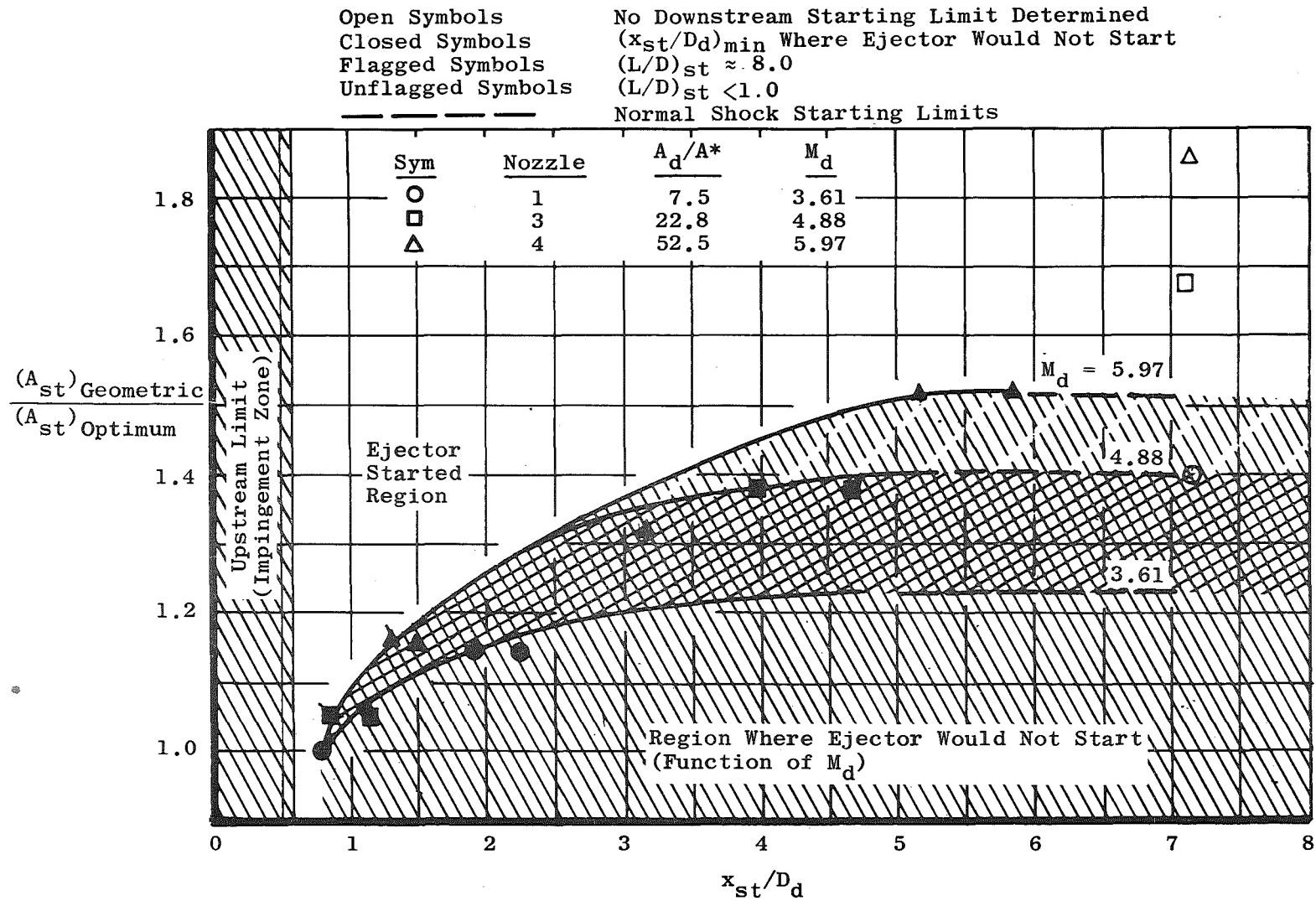
Fig. 21 Experimental Downstream Starting Limit